Processes setting the characteristics of sea surface cooling induced by tropical cyclones

Emmanuel M. Vincent, Matthieu Lengaigne, Gurvan Madec, Jérôme Vialard, Guillaume Samson, Nicolas C. Jourdain, Christophe E. Menkès, Swen Jullien

HAL Id: hal-00758293

https://hal.science/hal-00758293

Submitted on 8 Apr 2021

Processes setting the characteristics of sea surface cooling induced by tropical cyclones

Emmanuel M. Vincent,[1] Matthieu Lengaigne,[1] Gurvan Madec,[1,2] Jérôme Vialard,[1] Guillaume Samson,[1] Nicolas C. Jourdain,[3] Christophe E. Menkes,[1,4] and Swen Jullien[5]

[1]   A 1/2° resolution global ocean general circulation model is used to investigate the processes controlling sea surface cooling in the wake of tropical cyclones (TCs). Wind forcing related to more than 3000 TCs occurring during the 1978–2007 period is blended with the CORE II interannual forcing, using an idealized TC wind pattern with observed magnitude and track. The amplitude and spatial characteristics of the TC-induced cooling are consistent with satellite observations, with an average cooling of ∼1°C that typically extends over 5 radii of maximum wind. A Wind power index (*WPi*) is used to discriminate cooling processes under TCs with high-energy transfer to the upper ocean (strong and/or slow cyclones) from the others (weak and/or fast cyclones). Surface heat fluxes contribute to ∼50 to 80% of the cooling for weak *WPi* as well as away from the cyclone track. Within 200 km of the track, mixing-induced cooling increases linearly with *WPi*, explaining ∼30% of the cooling for weak *WPi*s and up to ∼80% for large ones. Mixing-induced cooling is strongly modulated by pre-storm oceanic conditions. For a given *WPi*, vertical processes can induce up to 8 times more cooling for shallow mixed layer and steep temperature stratification than for a deep mixed layer. Vertical mixing is the main source of rightward bias of the cold wake for weak and moderate *WPi*, but along-track advection becomes the main contributor to the asymmetry for the largest *WPi*s.

1.   Introduction

[2]   The ocean surface can cool by up to 10°C in the wake of tropical cyclones [*Chiang et al.*, 2011]. Such cooling was until recently mostly documented from ship measurements [*Leipper*, 1967], bathythermographs [*Shay et al.*, 1992] and buoy arrays [*Cione et al.*, 2000; *D'Asaro*, 2003]. The availability of satellite microwave sea surface temperature (SST) measurements, which are less sensitive to masking by clouds than infrared measurements [*Wentz et al.*, 2000], now allows a more extensive description of the SST response in several TC case studies [e.g., *Lin et al.*, 2005; *Chiang et al.*, 2011]. *Lloyd and Vecchi* [2011] describe TC-induced cooling at the global scale for the entire microwave satellite period. Their study reveals that the cold wake amplitude increases monotonically with the cyclone intensity up to category 2 but saturates for larger TC wind forcing. This result led the authors to assume that oceanic feedbacks could inhibit intensification of cyclones.

[3]   Because TCs draw their energy from evaporation at the ocean surface [*Emanuel*, 1986, 2003], sea surface temperature (SST) changes under the storm's eye can negatively feed back on cyclone intensification, as suggested by observational [*Cione and Uhlhorn*, 2003; *Kaplan and DeMaria*, 2003] and modeling results [*Schade and Emanuel*, 1999; *Bender and Ginis*, 2000; *Shen and Ginis*, 2003; *Schade*, 2000]. Among other influences–such as the storm's inner core dynamics or the structure of the synoptic-scale environment–processes that control the upper-ocean temperature under the TC remain one of the major uncertainties for improving TC intensity forecasts [*Marks et al.*, 1998].

[4]   Dominant processes in the oceanic response to TCs have mainly been discussed through cases studies in both observations [*Sanford et al.*, 1987; *D'Asaro*, 2003; *D'Asaro et al.*, 2007] and models [*Price*, 1981; *Morey et al.*, 2006; *Chiang et al.*, 2011; *Huang et al.*, 2009; *Chen et al.*, 2010]. These studies show that three main processes control SST fluctuations under TCs: oceanic vertical mixing, advection and air-sea heat exchange. The upper ocean cooling is primarily controlled by the entrainment of cold water from the thermocline into the mixed layer through vertical mixing,

[1]LOCEAN, IRD/CNRS/UPMC/MNHN, Paris, France.
[2]NOC, Southampton, UK.
[3]LEGI, CNRS/UJF/INPG, Grenoble, France.
[4]IRD, Noumea, New Caledonia.
[5]LEGOS, IRD/CNRS/UPS, Toulouse, France.

principally generated by the vertical shear of horizontal currents [*Pollard et al.*, 1973; *Price*, 1981; *Huang et al.*, 2009]. This entrainment mixing accounts for about 80% of the SST drop in TCs wakes [*Price*, 1981; *Sanford et al.*, 1987; *Shay et al.*, 1992; *Huang et al.*, 2009], but its contribution to the total cooling varies depending on the case study considered, from 70% in the case of TC Gilbert [*Jacob et al.*, 2000] to more than 90% in the case of TC Frances [*D'Asaro et al.*, 2007] or TC Gloria [*Bender et al.*, 1993]. Vertical mixing also seems to be responsible for the asymmetry of the cold anomaly with respect to the TC translation direction. Most intense inertial oscillations (and associated vertical shear) are indeed generated to the right (left) of the track in the Northern (Southern) Hemisphere, where TC winds rotate in the same direction as inertial currents, thus increasing the energy transfer to these currents [e.g., *Price*, 1981].

[5] Although of secondary importance, enhanced surface heat fluxes and advection processes also contribute to the TC-induced cooling. Evaporation (latent heat) dominates TC-related heat fluxes, while sensible, shortwave, longwave and precipitation-related fluxes play a lesser role [*Jacob et al.*, 2000; *Huang et al.*, 2009]. A coupled simulation of Hurricane Dennis revealed that air-sea heat exchanges were responsible for a widespread cooling of the sea surface and largely contributed to the total cooling far from the TC track for this cyclone [*Morey et al.*, 2006]. While cyclone-induced vertical suction cools the subsurface ocean near the cyclone track (S. Jullien et al., Impact of tropical cyclones on the South Pacific Ocean heat budget, submitted to *Journal of Physical Oceanography*, 2011), the effect of water advection on the structure of surface temperature anomalies requires further description. Indeed, horizontal advection has been shown to be locally important and it is suggested that it modulates the spatial pattern of the cold wake [*Huang et al.*, 2009; *Chen et al.*, 2010] as well as its asymmetry [*Greatbatch*, 1983].

[6] Most of the aforementioned studies investigate the mechanisms controlling the cold wake characteristics for case studies of individual or a limited number of TCs. Although vertical mixing was identified as the major contributor to the cooling around the TC eye, the respective contribution of each process to the observed cooling is shown to vary from one cyclone to another. The heat balance has also generally been examined in the region of maximum cooling or at a few points sampled by moored instrumentation of drifting buoys, while the cyclone-induced cooling often extends over hundreds of kilometers. A systematic study of the processes controlling the SST anomaly off the cyclone core region is however still missing [*D'Asaro et al.*, 2007].

[7] Past case studies have illustrated the influence of sub-surface oceanic background conditions on the TC-induced SST signature [*Shay et al.*, 2000; *Cione and Uhlhorn*, 2003; *Jacob and Shay*, 2003; *Shay and Brewster*, 2010]. Further support for sub-surface oceanic control of the amplitude of the TC-induced cooling has recently been provided on a global scale [*Lloyd and Vecchi*, 2011; E. M. Vincent et al., Assessing the oceanic control on the amplitude of sea surface cooling induced by tropical cyclones, submitted to *Journal of Geophysical Research*, 2011]. Vincent et al. (submitted manuscript, 2011) show that the widely varying

characteristics of upper-ocean pre-cyclone stratification can modulate the amplitude of TC-induced cooling by up to an order of magnitude for a given level of TC wind energy input to the upper ocean, but processes responsible for this modulation still need to be assessed.

[8] Because detailed observations under TCs are scarce, modeling offers a promising alternative to perform such an investigation. A few modeling studies [*Liu et al.*, 2008; *Sriver and Huber*, 2010; *Scoccimarro et al.*, 2011] have already performed global ocean simulations including TCs forcing. Using a simplified four layer ocean model forced by idealized hurricane wind forcing, *Liu et al.* [2008] estimated the rate of mechanical energy input to the world ocean induced by TCs. *Sriver and Huber* [2010] evaluated the influence of TCs on the mean ocean state and poleward heat transport from a global ocean general circulation model simulation in which they prescribe TC winds estimated from high resolution satellite wind data. None of these studies, however, investigated the processes involved in TC-induced cooling.

[9] The aim of this study is to characterize surface temperature response to TCs at a global scale, and to quantify how the related processes depend on TCs characteristics and oceanic background conditions. To that end, we forced a global ocean model with a modified version of CORE II forcing [*Large and Yeager*, 2009] including an analytic formulation of two-dimensional TC winds along observed TC tracks between 1978 and 2007. High-resolution data from satellite scatterometers do not provide reliable estimates for wind larger than 50 m s^{-1} and are only available from 2000 onward [*Brennan et al.*, 2009]. Our approach has the advantage of covering the entire range of TC intensities over a 30 years period, hence providing a large database of simulated ocean responses to more than 3000 TCs, with the caveat being that wind spatial structure for each individual cyclone is less accurate than satellites estimates.

[10] The paper is structured as follows. Section 2 describes the observed data set used in this study, the model configuration and the proposed modeling strategy to account for TC wind forcing. Section 3 validates our numerical experiment from statistical comparison of the simulated cold wakes to satellite estimates. The main processes that control the cooling, as well as their dependency to the cyclone wind power, distance to the track and oceanic background state are discussed in section 4. Section 5 provides a summary of our results as well as a discussion of their implications.

2. Data Sets and Methods

2.1. Observed Data Sets

2.1.1. Ocean Sub-Surface Temperature

[11] The depth of the mixed layer (ML) and the upper ocean thermohaline stratification are two important parameters controlling the response of near-surface ocean to the atmospheric forcing [*Jacob and Shay*, 2003; Vincent et al., submitted manuscript, 2011]. We use the recently updated mixed layer depth climatology of *de Boyer Montégut et al.* [2004], which includes ARGO profiles to September 2008 and temperature and salinity of the World Ocean Atlas 2009 climatology (WOA09) [*Locarnini et al.*, 2010] to validate the model climatology.

2.1.2. Sea Surface Temperature (SST)

[12] We use a blend of Tropical Rainfall Measuring Mission (TRMM) Microwave Imager (TMI) and Advanced Microwave Scanning Radiometer AMSR-E SST daily data set (http://www.ssmi.com/sst/microwave_oi_sst_data_description.html) to characterize the observed SST response to TCs over the 1998–2007 period. Despite its inability to retrieve SST data under heavy precipitation [Wentz et al., 2000], TMI and AMSR-E offer the advantage of being insensitive to atmospheric water vapor and provide accurate observations of SST beneath clouds, a few days before and after TC passage. The inner-core cooling (i.e., cooling under the eye) cannot be assessed confidently with TMI-AMSR; data are most of the time missing in a 400 km radius around the current TC position. This data set however provides a reliable estimate of the cooling in the TCs wake, data being typically available 1 to 2 days after TC passage. It has however to be noted that the cooling amplitude in the TCs' wake may not be fully captured by this data set, especially for slow moving TCs.

2.1.3. Tropical Cyclone Position and Strength

[13] Observed TC position and strength are derived from the International Best Track Archive for Climate Stewardship (IBTrACS) [Knapp et al., 2010]. In this study, we focus on the 1978–2007 period, over which worldwide satellite coverage provides the position and estimated maximum wind speed every 6 h for more than 3000 TCs. The maximum wind speed value characterizing the TC strength is taken as the 10-minute averaged wind at 10 meters.

2.2. Methodology to Monitor the Ocean Response to TCs

[14] To characterize the ocean response to TCs, the mean seasonal cycle of each field collocated to TC tracks is first subtracted from model and observations; TC track locations, available at 6-h intervals, are then used to retrieve the ocean response to TCs through these fields (SST, ML currents and ML heat budget terms). Those data are projected along and across track axes, with cross-translation axis oriented to the right (left) of the moving TC in the Northern (Southern) Hemisphere. A fixed radius of 200 km (about 3–4 RMW) around each TC-track position is used to characterize the maximum cooling amplitude. This region encompasses a crucial area where SST is known to influence TC intensity [Cione and Uhlhorn, 2003; Schade, 2000].

[15] The reference unperturbed pre-storm SST conditions (SST_0) is defined as the 7-day average from 10 to 3 days before the TC passage. The inner-core SST (SST_{eye}) is defined as the daily average 12 hours before to 12 hours after the storm passage. The SST in the wake of the TC (SST_{CW}) is defined as the 3-day average starting 24 hours after the storm passage. The amplitude of the SST response is characterized by the cooling amplitude in the cold wake (CW) as $\Delta T_{CW} = SST_{CW} - SST_0$ and the cooling amplitude in the inner-core region as $\Delta T_{eye} = SST_{eye} - SST_0$. We will see in section 3 that these choices for spatial and temporal averaging are justified by the observations and modeling results. Because satellite observations do not offer reliable estimates for SST_{eye}, only ΔT_{CW} is validated against satellite estimates. However, results for ΔT_{eye} in the model will also be discussed owing to the importance of temperature right under the TC eye on cyclone intensity [Cione and Uhlhorn, 2003]. Note that while the definitions above are generally

reasonable for most storms, they may induce some errors for very slow (where our definition of SST_0 or SST_{CW} may capture some of the eye signal) or very fast moving storms.

[16] Following Vincent et al. (submitted manuscript, 2011), two variables are used in this study to diagnose the amplitude of the TC atmospheric forcing and the subsurface oceanic background conditions. The Wind Power index (WPi) characterizes the strength of the TC forcing. This index integrates in a single measure several parameters known to influence the cold wake amplitude: storm size, maximum winds and translation speed of the TC. The WPi builds on the Power Dissipated by friction at the air-sea interface (PD) [Emanuel, 2005] that is a good proxy of the kinetic energy transferred from the winds to the ocean surface currents (Vincent et al., submitted manuscript, 2011). The PD is calculated for each cyclone track position as

$$PD = \int_{t_o}^{t_c} \rho \, C_D \mathbf{V}^3 \, dt,$$

and the WPi writes as follows:

$$WPi = [PD/PD_0]^{1/3},$$

where $|\mathbf{V}|$ is the local magnitude of surface wind, C_D the dimensionless surface drag coefficient, ρ the surface air density, t_o the time when a cyclone starts influencing the considered location and t_c the current time; $PD_0 = \int_{t_o}^{t_c} \rho C_D |\mathbf{V}_0|^3 dt$ is a normalization constant corresponding to a weak storm with a translation speed of 7 m.s^{-1} (25 km.h^{-1}) and a maximum 10-minute averaged wind speed of 15 m.s^{-1} (the wind speed defining a Tropical Depression: the weakest cyclonic system classified).

[17] WPi is a proxy of the amount of kinetic energy available for mixing under the storm (Vincent et al., submitted manuscript, 2011). As the cooling mainly results from mixing induced by vertical shear of oceanic currents [Price, 1981], this is a pertinent variable to describe the resulting ocean cooling. We use the term 'power' to refer to a TC's WPi while the term 'intensity' is kept to comment the maximum wind speed (V_{max}) for consistency with most previous studies.

[18] The magnitude of the cooling also depends on the ocean background conditions (i.e., shallow and steep or deep and diffuse thermocline). We use the Cooling Inhibition index (CI) introduced by Vincent et al. (submitted manuscript, 2011) to describe that effect. The definition of the CI is based on the physical process responsible for the cooling: conversion of kinetic energy to potential energy by vertical mixing. Vincent et al. (submitted manuscript, 2011) show that the amplitude of the cooling is proportional to the cube root of the potential energy change. CI is hence defined as the cube root of the potential energy necessary to produce a 2°C cooling via a heat-conserving vertical mixing. This quantity can easily be computed from any available pre-storm temperature and salinity profiles. It measures the inhibition of mixing-induced ocean surface cooling by the ocean background state. Vincent et al. (submitted manuscript, 2011) showed that TC-induced variations in our simulation are largely a function of WPi and CI, with CI modulating the cooling amplitude by up to an order of magnitude for a given WPi.

2.3. Model Setup

2.3.1. Model Configuration

[19] The model configuration used here is built from the "Nucleus for European Modeling of the Ocean" ocean/sea-ice numerical framework (NEMO v3.2) [*Madec*, 2008]. This configuration (known as ORCA05) uses a tripolar, quasi-isotropic grid with a nominal resolution of $1/2°$ (i.e., cell size $\sim$50 km in the tropics). It has 46 vertical levels, with 10 levels in the upper 100 m and 250 m resolution at depth. Partial filling of the deepest cells is allowed [*Bernard et al.*, 2006; *Barnier et al.*, 2009]. Such a configuration has been shown to successfully reproduce tropical ocean variability at time scales ranging from intra-seasonal to inter-annual [*Penduff et al.*, 2010].

[20] The mixed layer dynamics is parameterized using an improved Turbulent Kinetic Energy (TKE) closure scheme [*Madec*, 2008] with a Langmuir cell [*Axell*, 2002], a surface wave breaking parameterization [*Mellor and Blumberg*, 2004] and an energetically consistent time and space discretization [*Burchard*, 2002; *Marsaleix et al.*, 2008]. Additional subgrid-scale mixing parameterizations include a bi-Laplacian viscosity and an iso-neutral Laplacian diffusivity. For tracer advection, a total variance dissipation scheme —a second-order, two-step monotonic scheme with moderate numerical diffusion— is used [*Lévy et al.*, 2001].

[21] In this configuration, the mixed layer depth is defined as the depth where the vertical density is 0.01 kg m^{-3} higher than the surface density. The different terms contributing to the heat budget in the ocean mixed layer (ML) are calculated online and stored. As with *Vialard et al.* [2001], the ML temperature evolution equation reads

$$\partial_t \bar{T} = \underbrace{-\langle u\partial_x T + v\partial_y T + w\partial_z T \rangle}_{(a)} + \underbrace{\langle D_l(T) \rangle}_{(b)} - \underbrace{\frac{1}{h}\frac{\partial h}{\partial t}(\bar{T} - T|_{z=h})}_{(c)}$$

$$+ \underbrace{\frac{(\kappa\partial_z T)|_{z=h}}{h}}_{(d)} + \underbrace{\frac{Q^* + Q_s(1 - F(z = h))}{\rho_o C_p h}}_{(e)}, \quad (1)$$

where $\bar{T} = \langle T \rangle \approx SST$ is the mean temperature in the ML, T the temperature, (u, v, w) the three components of ocean currents, $D_l(T)$ the lateral diffusion operator, κ is the vertical diffusion coefficient, h the time varying MLD, $C_p = 4.10^3$ J. K^{-1}. kg^{-1} is the specific heat of seawater, and ρ_o is a reference density. Brackets denote the vertical average over h. Term a is the advection, term b is the lateral diffusion, term c is the entrainment/detrainment at the ML base, term d is the vertical diffusion flux at the ML base and term e is heat flux storage in the ML (with Q_s the solar heat flux and Q^* the non-solar heat fluxes: sensible, latent, radiative heat fluxes; $F(z = h)$ is the fraction of surface solar irradiance that penetrates below the mixed layer.

[22] We will use this heat budget calculation to infer the respective contribution of these processes to the amplitude of the TCs-induced cooling. The term b for lateral diffusion is negligible in the wake of TCs. In the following, term b is neglected, terms c and d are grouped together in a vertical processes term and referred to as MIX; term e is the surface forcing term is referred to as FOR; term a is the advection term is referred to as ADV. In fact ADV is almost only the horizontal advection term, the vertical one being always

negligible. Indeed, the temperature equation (1) is a budget over the time varying ML (defined on a density criterion), the base of which is a surface moving up and down with vertical currents. In this Lagrangian framework, it is largely the MIX term that operates for exchanging heat between the ML and subsurface layers. The Eulerian vertical advection is known to be an important contributor to the ocean cooling under TCs [*Greatbatch*, 1985; *Yablonsky and Ginis*, 2009; Jullien et al., submitted manuscript, 2011], but its effect on ML temperature only appears indirectly in (1): it contributes to term d by both reducing the MLD (thus increasing shear-induced mixing and so κ), and tightening the stratification at the base of the ML (thus increasing $\partial_z T$).

[23] To quantify the relative contribution of all processes to the cooling magnitude, each term of the ML heat budget is integrated starting 10 days prior to TC passage. The cooling magnitude ΔT_{CW} and ΔT_{eye} associated with each term are then calculated as explained in part 2.2.

2.3.2. Model Surface Boundary Conditions

[24] The three simulations performed in this paper use the atmospheric data sets and formulations proposed by *Large and Yeager* [2009] as surface boundary conditions. This approach was developed in the design of the "coordinated ocean-ice reference experiments (COREs)" program [*Griffies et al.*, 2009] and is referred to as COREII forcing. The forcing data sets presented by *Large and Yeager* [2009] are based on NCEP/NCAR reanalysis products over the 1958–2007 period combined with various satellite data sets. Turbulent fluxes are computed from bulk formulae as a function of the prescribed atmospheric state and the simulated ocean surface state (SST and surface currents). Data are provided at six-hourly (wind speed, humidity and atmospheric temperature), daily (short- and long-wave radiation) and monthly (precipitation) resolution, with inter-annual variability over the 1978–2007 period, except for river run-off that remains climatological. To avoid an artificial model drift, the sea surface salinity is damped towards monthly-mean climatological values with a piston velocity of 50 m per 300 days [*Griffies et al.*, 2009]. It must be noted that the *Large and Yeager* [2009] formulation of the forcing accounts for the observed saturation at strong winds [*Donelan et al.*, 2004], the dimensionless surface drag coefficient (C_D) is bounded to a value of 2.34×10^{-3} for winds greater than 33 m s^{-1}. The use of a threshold on the surface drag coefficient C_D also implies a similar bound on the latent heat exchange C_E and sensible heat exchange C_H coefficients (calculated from C_D following *Large and Yeager* [2009, equations 9 and 11]).

[25] The model starts from an ocean at rest initialized with temperature and salinity fields from the World Ocean Atlas 2005 [*Locarnini et al.*, 2010]. It is then spun up for a 30-year period using the interannual 1948–1977 COREII forcing. The final state is then used to start the simulations described below (which are run over 1978–2007). The first of these experiments simply continues with the original COREII forcing, and will be referred to as COREII. As illustrated in Figure 1a, the COREII wind forcing contains weaker-than-observed TC wind signatures (TC-like vortices). These residual TCs signatures have been filtered out by applying a 11-day running mean to the zonal and meridional wind components of the original COREII wind forcing, within 600 km around each cyclone track position, with a linear
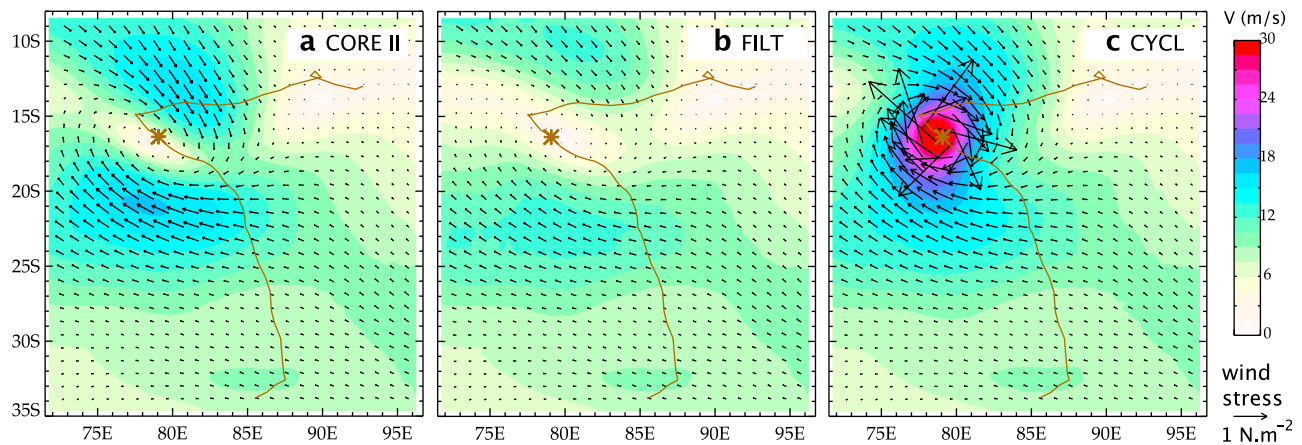
Figure 1. Wind module (shading) associated to the passage of TC Francesca at the position noted by a star (5 February 2002) in (a) CORE II, (b) FILT and (c) CYCL experiments. Black arrows are for the 1-day averaged wind stress magnitude.

transition from filtered to unfiltered winds between 600 and 1200 km. In this simulation (FILT), most of the TC-like vortex is suppressed (Figure 1b). It will therefore be our reference simulation for ocean response without TC.

[26] The third simulation, which is the main focus of this paper, is obtained by adding idealized TC wind forcing along cyclone tracks to the filtered COREII forcing. TC wind patterns are computed using the *Willoughby et al.* [2006] idealized vortex, which is based on a statistical fit to observed TC winds [*Willoughby and Rahn*, 2004]. This idealized wind pattern is computed at each model time step (36 min) using interpolated position and maximum wind speed of each cyclone from the 6-hourly IBTrACs database. This strategy ensures that both temporal evolution and spatial structure of the TC wind forcing are properly captured in the simulation. This procedure results in a simulation (CYCL) where TC wind magnitude is realistic (Figure 1c). Note that we chose not to take into account the translation speed of the storm in the wind vortex we added. Indeed, even if it is known to affect the wind asymmetry, *Samson et al.* [2009] have shown that it has a limited effect on the CW asymmetry and can be neglected. The validity of our methodology for simulating the ocean response to TCs will be further illustrated in the next section.

2.3.3. Model Resolution

[27] The 1/2° horizontal resolution employed in the present study may seem rather coarse compared to previous case studies simulating the ocean response to single TCs [e.g., *Yablonsky and Ginis*, 2009; *Halliwell et al.*, 2011]. Our strategy is to perform long-term global simulations that allow analyzing the ocean response to a large variety of TCs. This does not allow us to use eddy permitting ocean model due to computing cost limitations. A major requirement for realistic simulation of ocean response to TC is that the surface wind forcing accurately captures the maximum winds of the TC eyewall [*Halliwell et al.*, 2011]. We stress that the use of an analytic TC vortex allows us to avoid the pitfall of low atmospheric resolution that would smooth out the maximum winds. The remaining question is thus how the spatial sampling on the ocean grid will capture the TC surface forcing. We provide here a simple quantification of how horizontal resolution may affect our results by analyzing two

crucial processes of the ocean response to a cyclone wind forcing: vertical mixing and wind-induced upwelling [*Yablonsky and Ginis*, 2009]. The ability to force the former can be evaluated by considering the power dissipated (PD: a good proxy of the energy input to the ocean (Vincent et al., submitted manuscript, 2011) to which the shear-induced mixing is roughly proportional) while for the later, the Ekman pumping can be used as a mean proxy (vertical motion is an Ekman solution with a superimposed inertial oscillation; in the text, we use the term Ekman suction when explicitly referring to upward vertical motion). Figure 2 provides a comparison of these two quantities for a selected strong tropical cyclone (TC DORA; SS-Cat. 4; in the southwestern Indian Ocean in early 2007 [*Vialard et al.*, 2009]) computed for various grid resolutions ranging from 2° to 1/12°. The 1/2° resolution model used in our study is sufficient to provide a reasonable estimate of these two quantities and thus appears to be a good compromise between computational cost and accuracy. Compared to the 1/12°, it provides very similar results in terms of power dissipated. However, it underestimates the maximum upwelling amplitude near the cyclone's eye by about 30%. We will come back to this point in the discussion.

3. Characteristics of Modeled and Observed Cold Wakes

3.1. Validation of the Model Background State

[28] The mixed layer depth (MLD) and the Cooling Inhibition index (CI) are two important parameters involved in the amplitude of the SST response to TCs. The CI characterizes the efficiency of vertical mixing in cooling the ocean surface (Vincent et al., submitted manuscript, 2011) while the MLD controls the amplitude of the SST response to a given atmospheric heat flux forcing. Figure 3 shows these parameters for model and observations during the peak cyclonic season for both hemispheres (DJF for Southern Hemisphere and JJA for Northern Hemisphere). The model reproduces qualitatively the main features of both observed estimates of MLD and CI (Figure 3). The highest values of CI are found in the west Pacific warm pool where the thermocline is deep, while upwelling regions such as the eastern
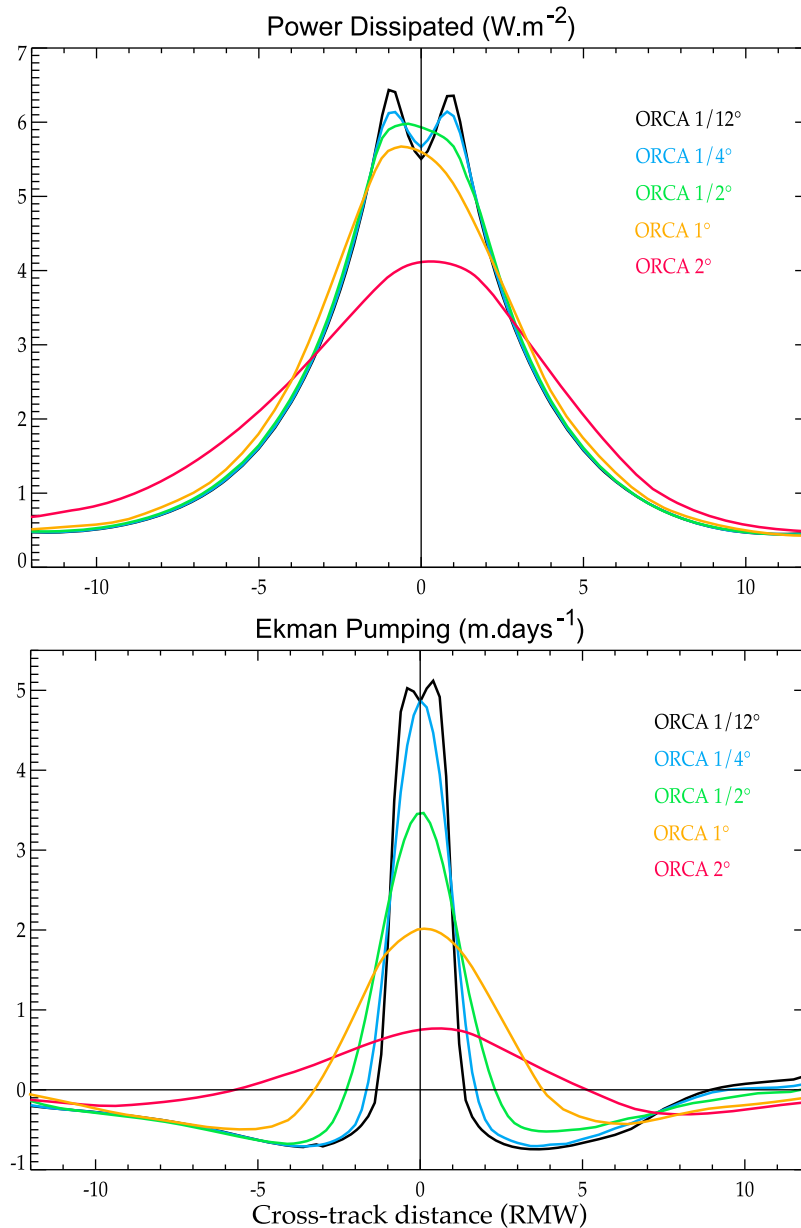
Figure 2. Comparison of average (a) power dissipated (W m^{-2}) and (b) Ekman pumping (m d^{-1}) for grids of increasing resolution (1/12°, black; 1/4°, blue; 1/2°, green; 1°, orange; 2°, red). These figures were obtained from reproducing category 4 TC DORA surface forcing (from 25 January to 7 February 2007) over different ocean grids. Cross section are averages of all cross sections for each 6-h track-position made in the averaged PD and cumulated Ekman pumping fields over the storm's lifetime.

equatorial Pacific or the Seychelles-Chagos thermocline ridge [e.g., *Vialard et al.*, 2009] are characterized by low CI. The model generally tends to underestimate CI, most notably in three cyclonic basins: northeastern and southwestern Pacific, northern Indian Ocean. This may lead to overestimated cooling response in those regions, especially in the northeastern Pacific where the mean CI value is rather low. Similarly, in those three regions, the mixed layer depth tends to be underestimated.

3.2. Amplitude of TC-Induced Ocean Response

[29] The efficiency of our experimental design to account for a realistic TC wind forcing is illustrated on Figure 4. The

figure displays a scatter plot of the amplitude of modeled against observed TC-induced cold wake amplitude (ΔT_{CW}) at individual locations for the three experiments discussed in section 2.4. The original COREII forcing contains weaker than observed TC-like vortices along the observed TC tracks, triggering weaker than observed sea surface cooling that saturate around $-1°C$ (Figure 4a). Filtering these vortices (FILT experiment) allows suppressing most of those weak cooling events (Figure 4b); further applying idealized TC wind along the observed tracks (CYCL experiment) allows a realistic simulation of the cold wake (CW) amplitude. In CYCL, there is a 0.71 correlation between modeled and observed TC-induced cooling magnitude at individual
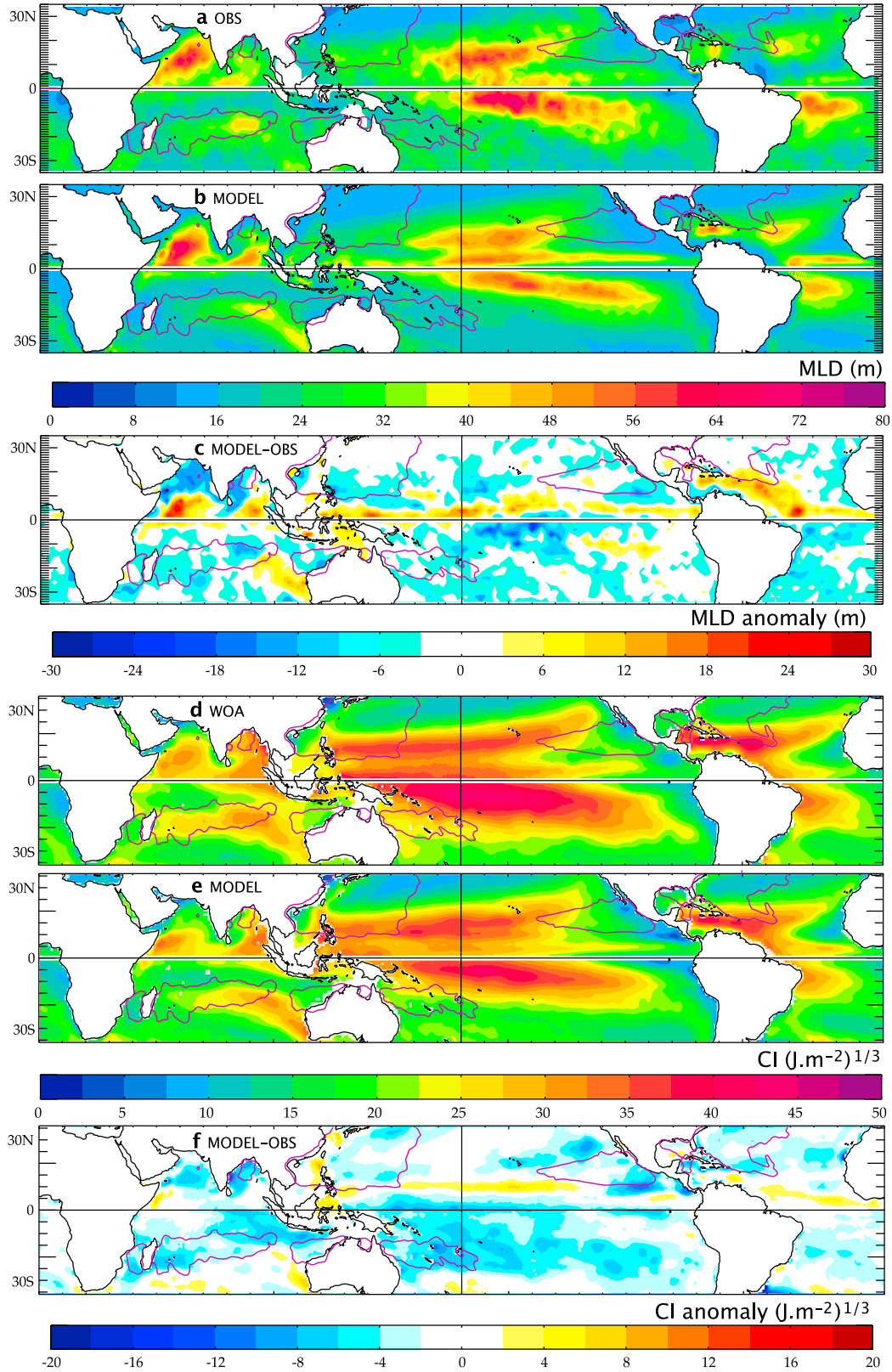
Figure 3. Climatological values for "cyclonic season" (DJF for the Southern Hemisphere and JJA for the Northern Hemisphere) of the mixed layer depth (a) observed [*de Boyer Montégut et al.*, 2004], (b) modeled in CYCL experiment and (c) difference between modeled and observed. (d–f) Same as Figures 3a–3c but for the cooling inhibition index (*CI*) (Vincent et al., submitted manuscript, 2011); in Figure 3d "observation" is from WOA09 database [*Locarnini et al.*, 2010]. The purple line reminds the regions of intense TC activity (average 1978–2007 *WPi* > 1).
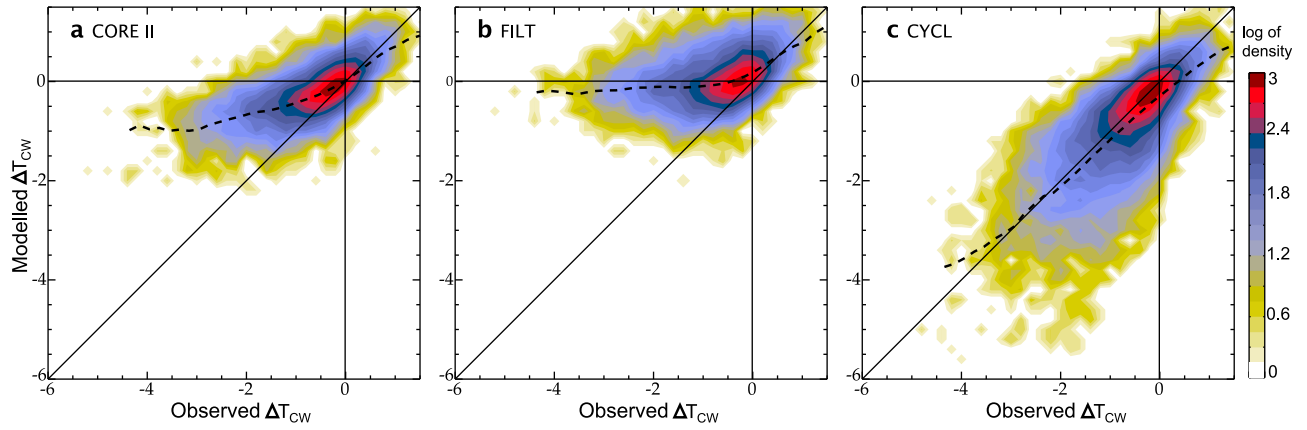
Figure 4. Probability density function of simulated versus observed cold wake amplitude averaged within 200 km of any cyclone position over the 1998–2007 period for (a) CORE II, (b) FILT and (c) CYCL experiments. ΔT_{CW} is calculated as the difference between the post-storm SST (averaged from 1 to 4 days after TC passage) minus the pre-storm SST (averaged from 10 days prior to 3 days prior TC passage). Dashed lines indicate the mean modeled cooling as a function of the observed one.

locations (Figure 4c), indicating that this simulation realistically samples the ocean response to TCs. Because the analytic cyclone wind field formulation is fitted to an average of observed cyclone wind radial profiles [*Willoughby and Rahn*, 2004], and because the underlying ocean state does not exactly match the observed one (biases, misplaced or missing oceanic eddies…), we however do not expect every simulated cold wake to perfectly match the corresponding observed one as indicated by the rather large spread observed on Figure 4c.

[30] The model also successfully reproduces the observed spatial distribution of the TC-induced cooling (Figure 5): the average cooling within TC-active regions is about 1°C in most basins, with maximum amplitude of about 2°C in the northwest Pacific region where most of the strongest TCs occur. The main model deficiency lies in the northeast Pacific basin where modeled average cooling is

overestimated by almost 1°C. This bias may be attributed to a shallower than observed thermocline in this region. As a result, the modeled CI underestimates the value from the World Ocean Atlas (Figure 3) in a region where its value is the lowest of all TC basins (CI value in JJA of 12 in the model against 18 $(J\,m^{-2})^{1/3}$ in observations in the region 120°W–80°W/5°N–20°N). The statistical model of Vincent et al. (submitted manuscript, 2011), that links the cooling amplitude to the CI and WPi suggests that such CI bias explains the ~1°C cooling bias in this region.

[31] In observations, the cooling magnitude monotonically increases with wind intensity up to TC category 2 of the Saffir-Simpson scale and then saturates from category 2 to 5 (Figure 6a), as discussed by *Lloyd and Vecchi* [2011]. The model reproduces reasonably well this feature, despite a slight overestimation of the cooling for the strongest cyclones with winds greater than 45 m s^{-1} (~0.3°C on
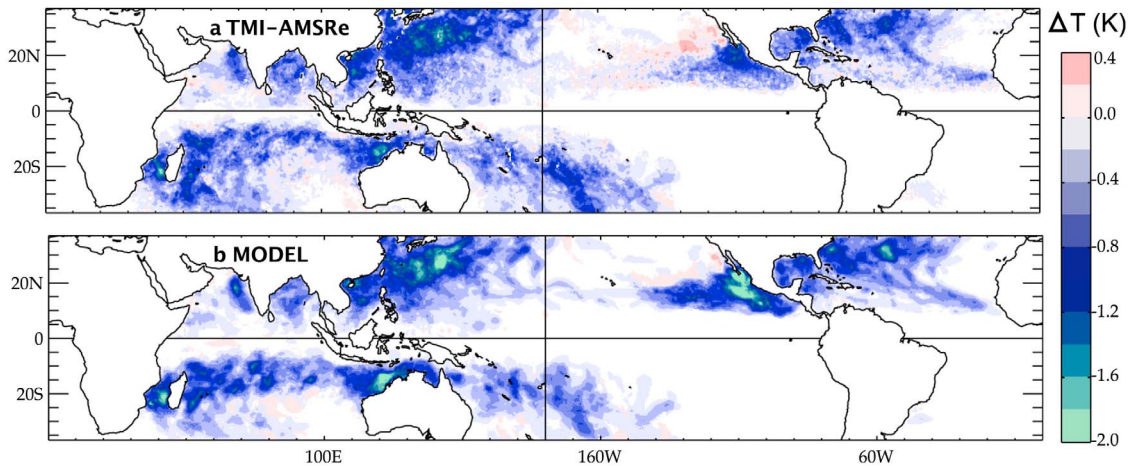

Figure 5. Spatial map of average cold wake amplitude over 1998–2007 for (a) TMI-AMSRe observations and (b) CYCL experiment. These maps are produced as follows: the maximum amplitude of ΔT_{CW} reached during a TC passage over each grid point within 200 km of each TC position are averaged for all TCs passing over the same grid point within the same TC season; these seasonal maps are then averaged over the 1998–2007 period.
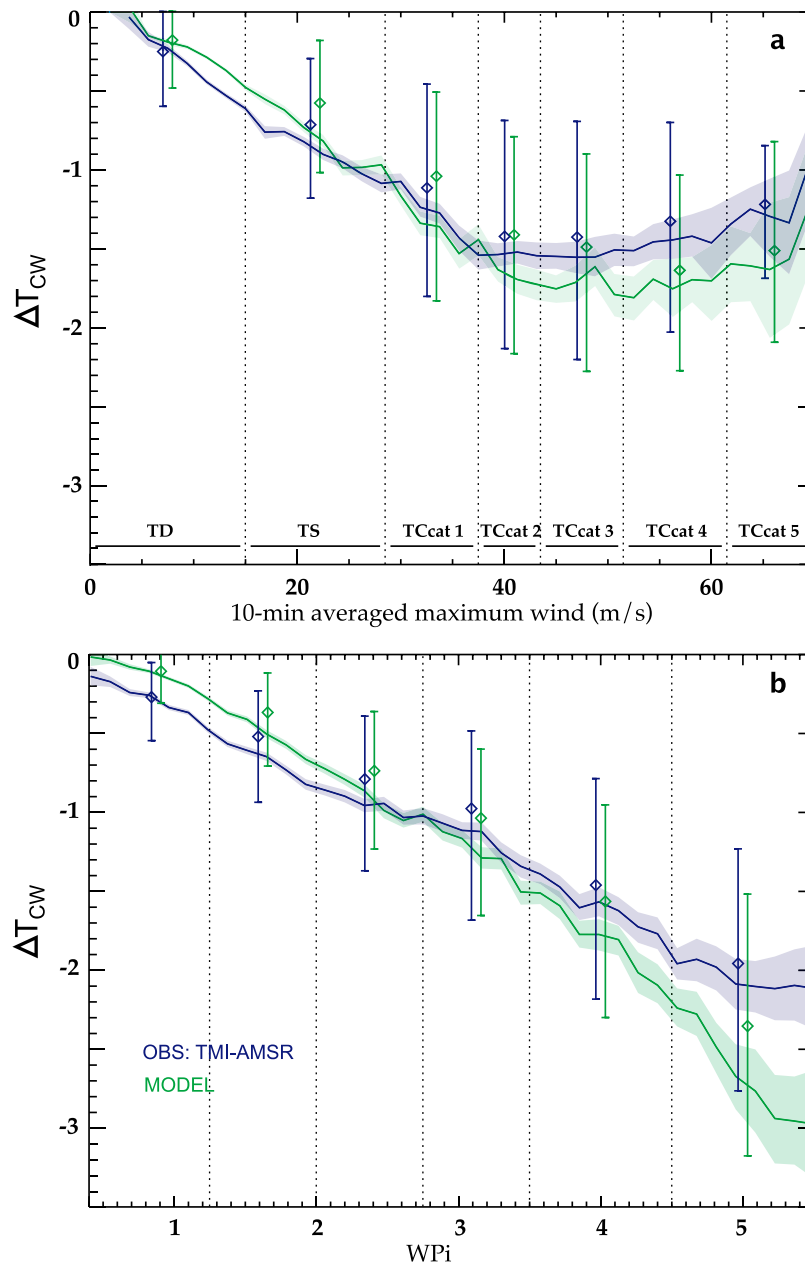
Figure 6. Mean observed and simulated cooling (a) as a function of 10-min averaged maximum wind speed (Saffir Simpson scale is reminded by the horizontal bars) and (b) as a function of the wind power index (*WPi*). Comparison is made for all TCs occurring during the 1998–2007 period. Shading indicates the 95% confidence level from a bootstrap test for the calculation of the average ΔT. Diamonds are for the median cooling per bin and vertical bar indicates the dispersion between the lower and upper quartiles per bin.

average). *Lloyd and Vecchi* [2011] interpreted this saturation as evidence of the ocean control on TCs: they suggest that, on average, the strongest observed cyclones are those for which pre-storm oceanic conditions do not allow large cooling.

[32] As discussed by Vincent et al. (submitted manuscript, 2011), the *WPi* is a proxy of the kinetic energy transferred to the upper ocean by the cyclone and is thus a better predictor of the cooling than the maximum wind of a TC. When displayed as a function of *WPi*, the mean cooling increases almost linearly and hardly saturates for the most intense wind power (Figure 6b). The model also reproduces the observed

linear increase of the cooling with the *WPi*, but with a clear overestimation (∼0.8°C) of the cooling for the highest range of *WPi* (>5). The modeled overestimation is partly related to the CI bias in the northeast Pacific that promotes stronger cooling than observed. Excluding the northeast Pacific basin in Figure 6b results in a 40% reduction of the cooling bias observed for *WPi* > 5 (bias of 0.5°C instead of 0.8°C). Another reason for this bias may also stem from data limitations: the highest *WPi* can only be reached for slow moving storms (typically translating at about 1.5 m s^{-1} for *WPi* above 5 (Vincent et al., submitted manuscript, 2011)); in this
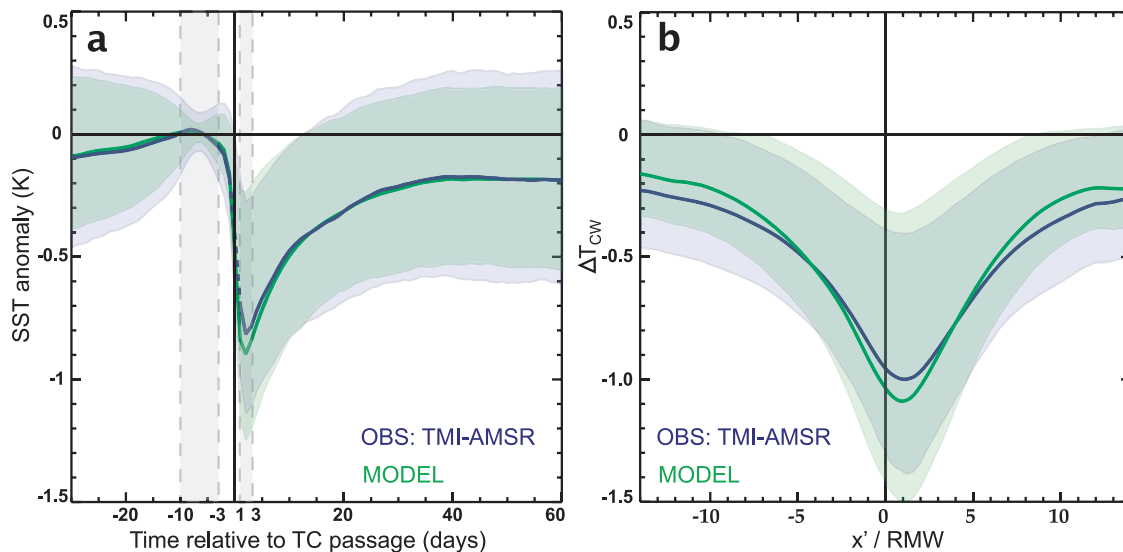
Figure 7. (a) Temporal evolution of the TC-induced cooling for model and observations. (b) Cross-track section of the cold wake. SST anomalies are calculated with respect to pre-storm SST (day-10 to day-3) and averaged for all TCs during the period 1998–2007. For Figure 7a, SST anomalies are averaged within 200 km radius of any TC track position. For Figure 7b, SST anomalies are averaged from 1 to 3 days after the cyclone passes and the x′ axis is normalized by the RMW value of the corresponding storm (the average RMW value for all TCs is 48 km). The x′ axis points to the right (left) of the track in the Northern (Southern) Hemisphere. Shading indicates the spread around the mean value, evaluated from the lower and upper quartiles.

case the TC covers ∼250 km in 2 days and part of the 200 km area over which the cooling is evaluated is still affected by precipitation: the cooling amplitude ΔT_{CW} is thus very likely underestimated by satellite observations. Excluding the slowest TCs (translation speed < 2.5 m s^{-1} (10 km h^{-1})) from Figure 6b and the northeast Pacific basin, the model overestimation for $WPi > 5$ is reduced by 75% (bias of 0.2°C instead of 0.8°C). The overestimation of modeled cooling to the strongest TCs may thus be linked to sampling issues rather than to inaccurate model representation of the ocean response.

3.3. Temporal Evolution and Spatial Extent of TC-Induced Ocean Response

[33] The CYCL experiment also captures accurately the temporal evolution of the average observed TC-induced cooling (Figure 7a). In both model and observation, SST averaged over a 200 km radius starts decreasing a few days before the TC reaches a given location (Day0) and maximum cooling occurs after the TC passage. Although maximum cooling appears to occur 1 to 2 days after the TC passage on Figure 7a for both model and observations, the exact timing of the maximum cooling after the TC passage cannot be confidently validated due to numerous missing satellite SST data around the time of TC passage. Figure 7a however illustrates that the decaying time scale of the cooling is accurately simulated, with about 40 days for the SST signal to disappear although the SST remains on average 0.2°C colder than pre-storm SSTs, as previously discussed by *Lloyd and Vecchi* [2011].

[34] The cold wake cross-track extent is also reasonably well simulated, despite a tendency to overestimate (underestimate) the cooling close (far) of the TC-track position (Figure 7b). On average, the maximum cooling

is shifted by one RMW on the inertial side (right for Northern Hemisphere, left for Southern Hemisphere in the frame of the moving TC) with respect to the TC-
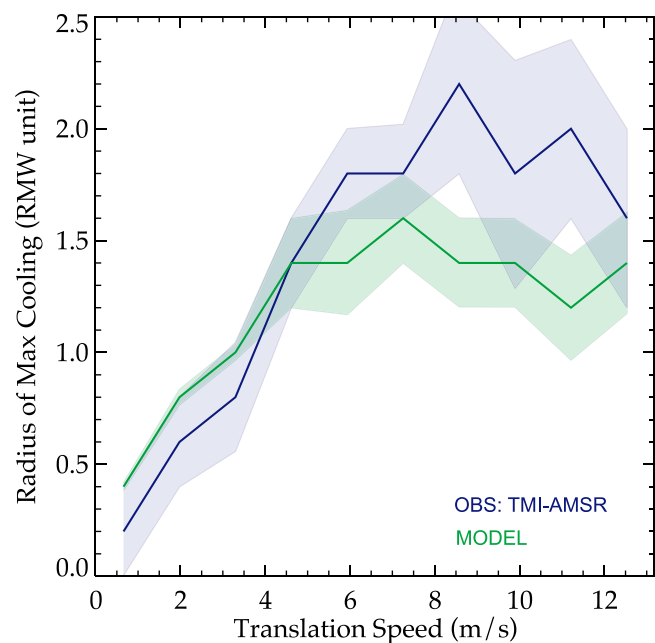

Figure 8. Cross-track distance between maximum cooling and the TC track in the wake of TCs as a function of storm translation speed. SST anomalies are calculated as the difference between the post-storm SST (averaged from 1 to 3 days after TC passage) minus the pre-storm SST (averaged from 10 days prior to 3 days prior TC passage).
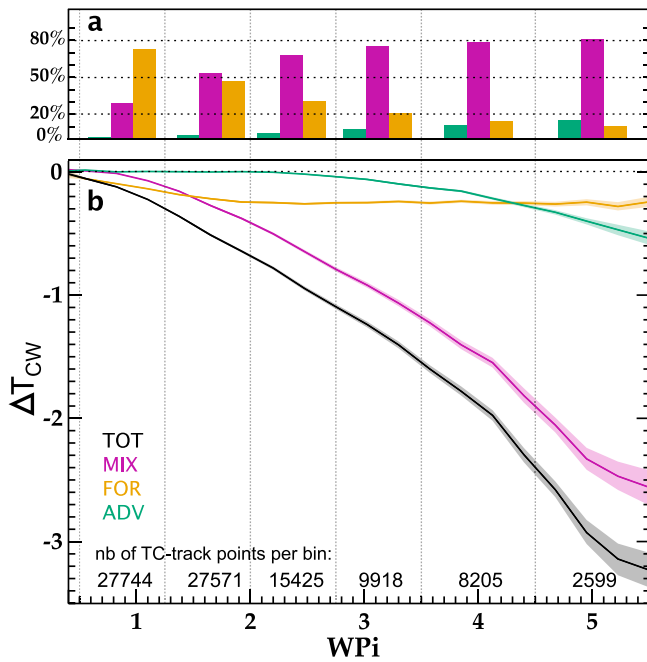
Figure 9. Mean amplitude of modeled cold wake ΔT_{CW} and respective contribution of vertical mixing (MIX), heat fluxes (FOR) and advection (ADV) to the total cooling as a function of the wind power index (*WPi*). (b) The absolute values and (a) the relative contribution of each process to the total cooling for 6 bins of increasing *WPi* are shown. The number of observations for each bin is indicated.

results [*Price*, 1981; *Samson et al.*, 2009]. *Price* [1981] attributed the more symmetric CWs to the effect of enhanced upwelling induced by slow moving storms that is centered under the TC track. This upwelling would allow entrainment to cool the ML more efficiently under the TC track that on the sides. The CW asymmetry is underestimated for fast moving cyclones in our simulation (Figure 8). Previous studies [*Greatbatch*, 1983; *Price et al.*, 1994; *Samson et al.*, 2009] suggest that the surface wind asymmetry due to the translation speed of the storm is of secondary importance to explain the asymmetric ocean response to TC forcing. The reason for the model biais may more likely be attributed to spatial/temporal grid sampling issues. Cyclone forcing is increasingly under-sampled by the model time-step (36 minutes) and spatial resolution at increasing translation speed: this may explain why the resonance mechanism is less well resolved for fast-moving storms.

[35] In the CYCL simulation, the amplitude of TC-induced ocean response, its temporal evolution, spatial extent and asymmetry with respect to the center of the track agree well with observed estimates. In the next section, we therefore use the model with some confidence to investigate the main oceanic and atmospheric processes controlling the characteristics of the TC-induced cooling. In the following, the analysis is extended to the full temporal coverage of the simulations (1978–2007) and the SST response is calculated from the difference between the CYCL and FILT simulations. This strategy, not applicable when comparing to observations, allows suppressing most of the variability unrelated to TCs (with the exception of the internal oceanic variability).

4. Oceanic and Atmospheric Processes Controlling the TC-Induced Cooling

4.1. Processes Controlling the Cooling Amplitude

[36] In agreement with previous studies, mixing at the base of the ML is the main process responsible for the

track position. Previous studies estimated this shift to be of 1 to 2 RMW [*Shay and Brewster*, 2010]. In both model and observations, the shift depends upon the translation speed of the storm (Figure 8), with slow moving storms triggering more symmetric CWs in agreement with previous
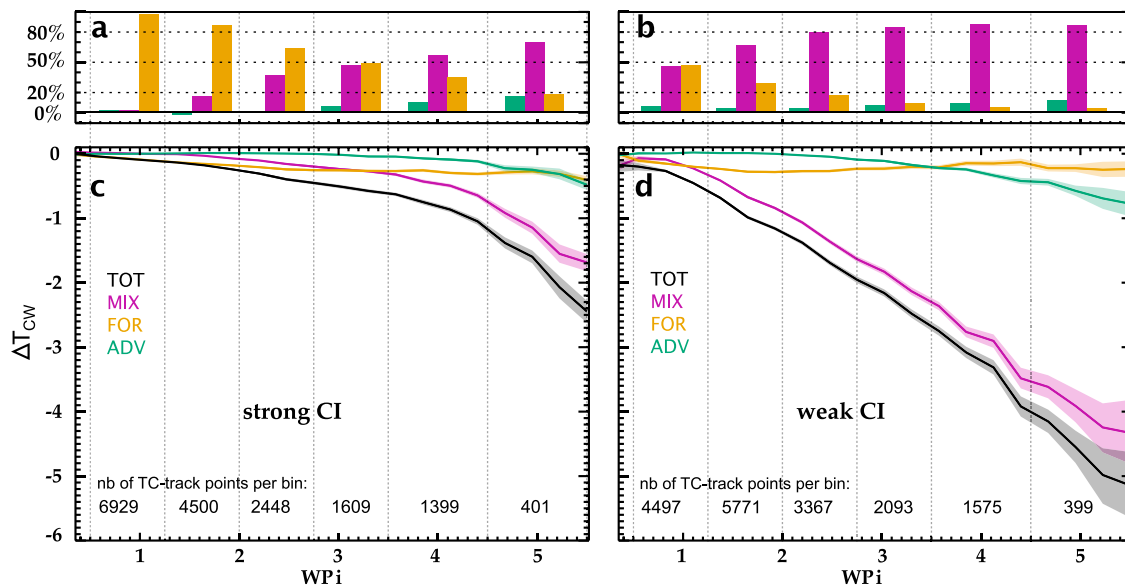

Figure 10. Same as Figure 9 but (a and c) for oceanic conditions that do not favor a strong cooling (strong cooling inhibition *CI* > 30) and (b and d) for oceanic conditions favorable to strong cooling (*CI* < 16).
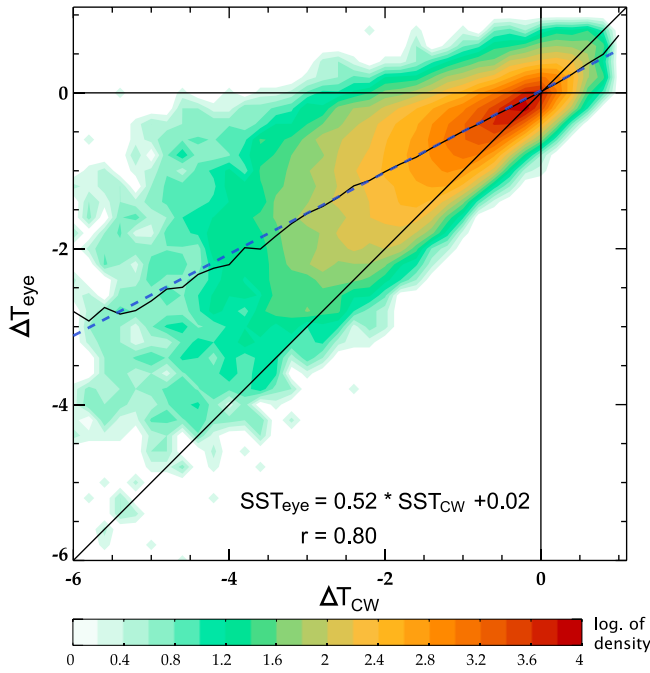
Figure 11. Probability density function of inner core cooling ΔT_{eye} versus cold wake ΔT_{CW} averaged within 200 km of any cyclone position. The plain line indicates the mean ΔT_{eye} as a function of ΔT_{CW}, while the dashed blue line is the linear fit of ΔT_{eye} onto ΔT_{CW}. The corresponding regression and correlation coefficients are provided.

TC-induced cooling, accounting for 56% of the SST signal within 200 km of the TC track on average for all TCs, while heat fluxes explain the largest part of the remaining signal (43%). The relative contribution of each term however strongly varies depending on the TC power (Figure 9). The relative contribution of mixing is shown to increase with *WPi*, evolving from ~30% of the total cooling for the weakest *WPi*s (*WPi* ≈ 1, i.e., weak and/or fast TCs) to 80% for the largest one (*WPi* ≥ 3, i.e., strong and/or slow TCs). This estimation of the mixing contribution for strong cyclonic forcing (i.e., slow and/or intense cyclones) is in broad agreement with previous estimates [*Shay et al.*, 1992; *Price*, 1981] that mainly investigated the SST response in the wake of intense TCs [*Jansen et al.*, 2010]. For low *WPi*, the weaker cooling is to a large extent explained (~70%) by enhanced surface fluxes associated with cyclone winds. The cooling amplitude induced by surface heat fluxes saturates around −0.25°C for *WPi* larger than 2, resulting in a decrease of the heat flux relative contribution to SST cooling for the strongest TCs (10%). Three main processes may explain this feature: (1) the saturation of heat exchange coefficients for the strongest winds, (2) the strong deepening of the mixed layer induced for the largest TC wind forcing (not shown) and (3) the limitation of latent heat flux by the increasingly cold SST anomaly in the wake of TCs of increasing power. Although of secondary importance, our analysis also reveals that advection, dominated by its horizontal component, significantly contributes to the cooling amplitude for the largest wind forcing (*WPi* > 3.5), accounting for more than 10% of the total cooling. As we

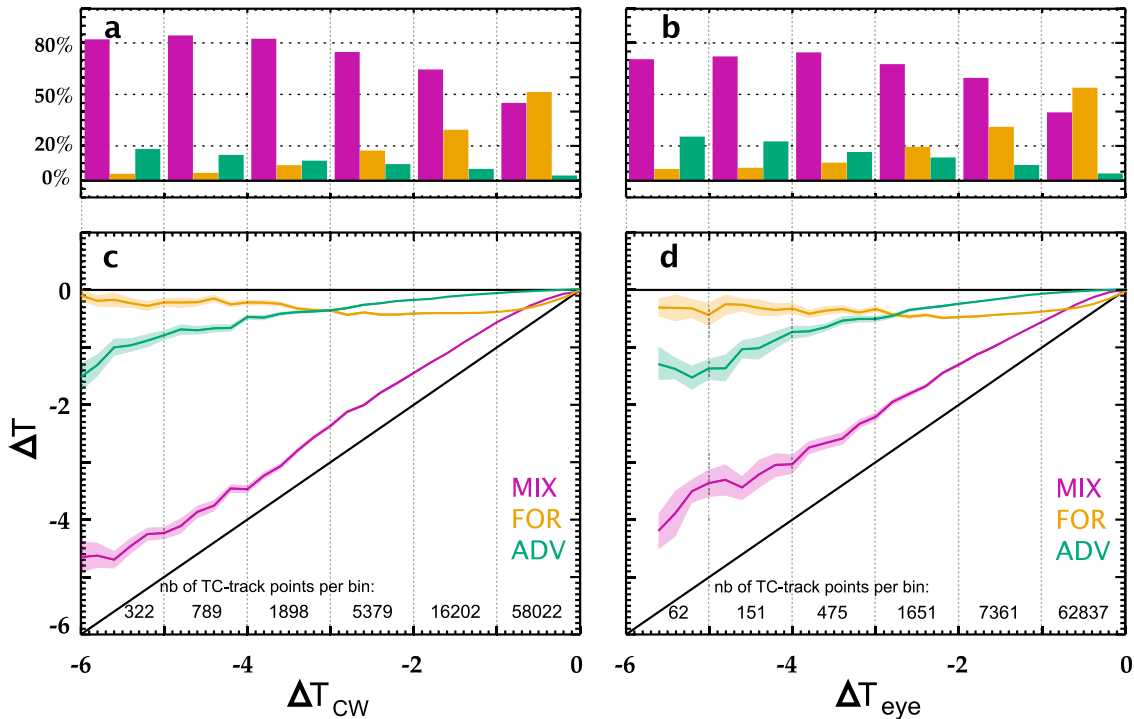**Figure 12.** Respective contribution of vertical mixing (MIX), heat fluxes (FOR) and advection (ADV) as a function of the total cooling amplitude for (a and c) cold wake ΔT_{CW} and (b and d) inner core cooling ΔT_{eye}. Figures 12c and 12d display absolute values, while Figures 12a and 12b display the relative contribution of each process to the total cooling for 6 bins of increasing cooling amplitude.
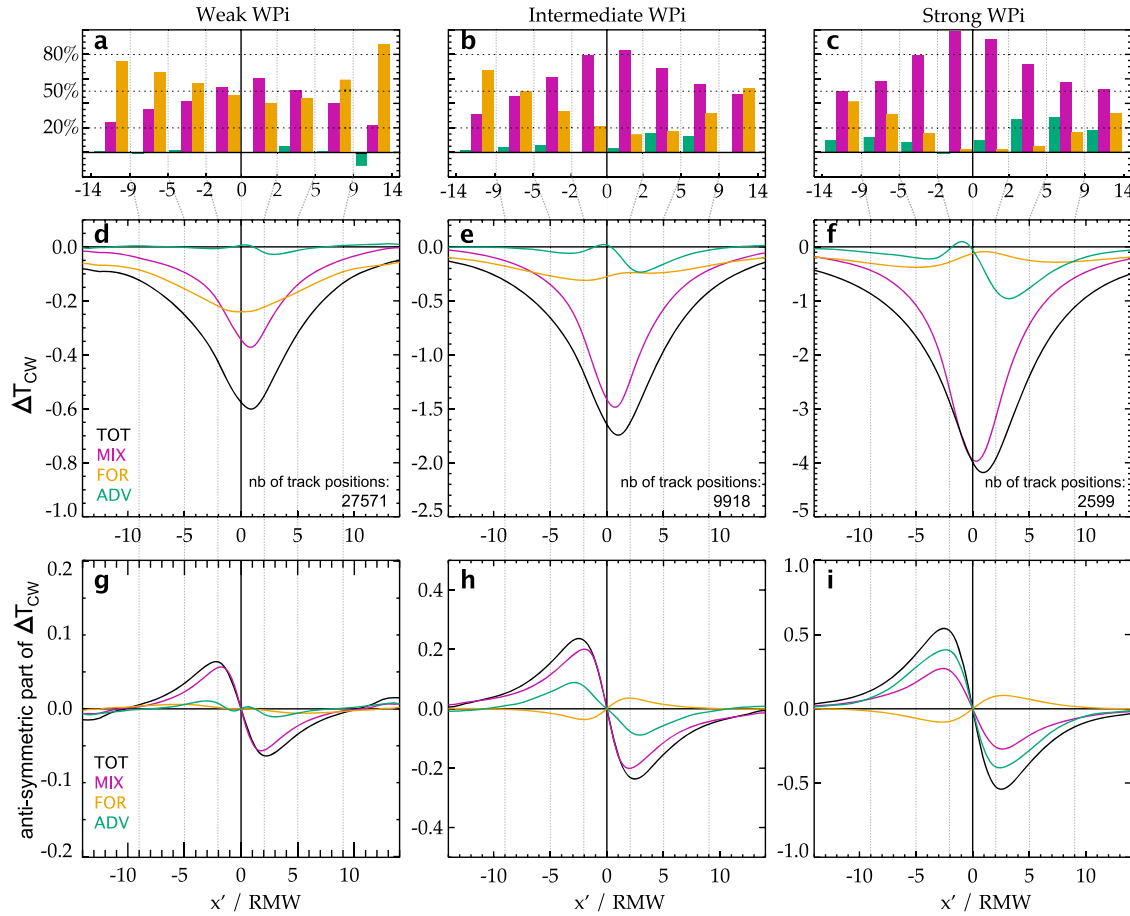
Figure 13. Cross-track sections of amplitude of modeled cold wake ΔT_{CW} and respective contribution of vertical mixing (MIX), heat fluxes (FOR) and advection (ADV) to the total cooling for three wind forcing categories: (a, d, and g) weak WPi (1.25 < WPi < 2), (b, e, and h) moderate WPi (2.75 < WPi < 3.5) and (c, f, and i) strong WPi (WPi > 4.5). Figures 13a–13c display the relative contribution of each process to the total cooling. Figures 13d–13f display absolute values, while Figures 13g–13i show the asymmetric part of the cooling. The x′ axis points to the right (left) of the track in the Northern (Southern) Hemisphere.

explained in section 2.3, vertical advection has a nearly negligible direct contribution to surface cooling in our Lagrangian framework (the bottom of the mixed layer is defined with a density criterion, and moves vertically with the vertical currents).

[37] The influence of subsurface oceanic conditions on the processes controlling the cooling is illustrated on Figure 10. As previously discussed by Vincent et al. (submitted manuscript, 2011), for a given wind power input, the cooling is greater for TCs occurring over oceanic conditions favorable for a strong cooling (low CI) than for those occurring over high CI. For WPi above 4.5, the cooling reaches 5°C for weak CI while it only reaches 2.5°C for large CI. This difference is mainly explained by the sensitivity of the mixing term to CI, while surface fluxes and advection have similar absolute contributions in both cases. Favorable oceanic conditions (i.e., shallow MLD and strong stratification below the mixed layer) increase the efficiency of vertical mixing in cooling the surface layers. For moderate WPi (2 < WPi < 3.5), mixing-induced cooling is on average −0.2°C (∼50% of the total) in the case of large CI, while it is 8 times larger for weak

CI with a −1.6°C cooling (∼80% of the total). As expected, a strong CI hence prevents the wind-induced mixing to entrain cold water into the ML except for the strongest and/or slowest TCs (WPi > 4.5).

[38] Investigating the processes responsible for the inner-core cooling is of great interest because this cooling is known to feedback onto the TC intensity [*Cione and Uhlhorn*, 2003]. In addition, this inner-core cooling is easily accessible in our model, while it is poorly sampled by observations (satellites being strongly affected by masking by clouds and intense rain). The amplitude of the inner-core cooling is on average half the amplitude of the cold wake (consistent with observations of *Cione and Uhlhorn* [2003]) but their respective amplitude are strongly correlated (0.8; Figure 11). The respective contribution of the processes explaining the inner core and cold wake are also globally similar (Figure 12). Surface fluxes and vertical mixing equally contribute to the weakest cooling in both the TC inner core and its wake. Mixing dominates the cooling greater than 3°C below the TC inner core, although its contribution is slightly weaker compared to cold wake cooling (70% against 80%). Lateral advection has on
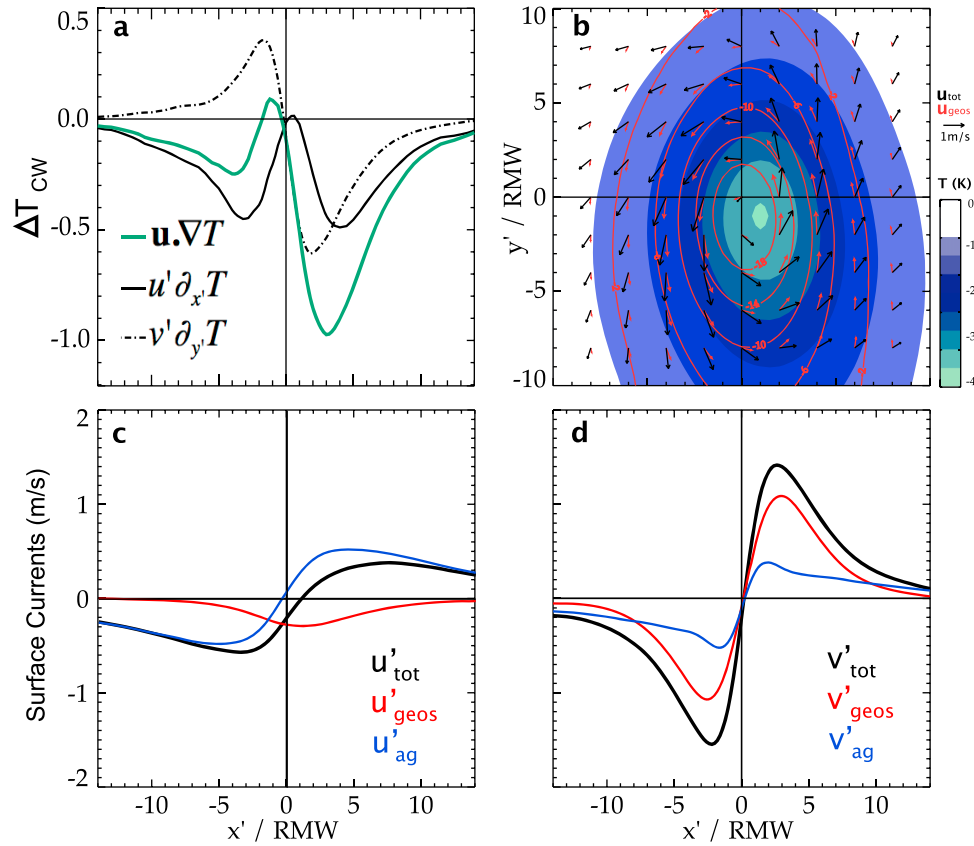
Figure 14. (a) Cross-track section of the contributions of total advection (green), advection by along track currents (dashed black) and cross track currents (plain black) to the total ML heat budget for strong *WPi* (*WPi* > 4.5). (b) Composite of CYCL-FILT SST (shading) SSH (red contours, in cm) surface currents (black arrows) and geostrophic currents (red arrows) in the frame of the moving TC averaged over day-1 to day + 3. Total, geostrophic and ageostrophic currents for the (c) cross-track components and (d) along-track components projected onto the cross-track direction axis x′. Ageostrophic component (blue) is simply calculated as the difference between total (black) and geostrophic (red) currents. Currents are averaged over the forced-stage period of the ocean response to the TC forcing (from day-1 to day + 3). The set of TCs used for this figure (*WPi* > 4.5) have an average translation speed of 2.6 m s^{-1}.

average a slightly larger relative contribution to the inner-core cooling than to the cold wake.

4.2. Processes Controlling the Cooling Spatial Extent

[39] We have so far investigated processes controlling the cooling averaged within 200 km of the TC track. This section investigates processes controlling the cooling away from the cyclone track, and its asymmetry with respect to the track.

[40] Irrespective of the cyclone power, the relative importance of mixing increases toward the eye, whereas the contribution of surface fluxes decreases (Figure 13). For the strongest wind power input, mixing induced cooling accounts for more than 80% of the total cooling within 2 RMW of the TC position, and dominates the cooling amplitude all along the cross track section (Figures 13c and 13f). For the weakest *WPi*s, mixing and heat flux induced cooling have a similar contribution near the cyclone track while heat fluxes dominate the cooling outside 2 RMW, explaining up to 80% of the cooling outside 9 RMW (Figures 13a and 13d).

[41] For strong *WPi*s, advection accounts for up to 30% of the total cooling at 2 to 5 RMW to the right of the TC track. Advection-induced cooling is increasingly asymmetric with increasing TC power (Figures 13g–13i). This asymmetry in advection is primarily associated to horizontal advection while vertical advection effect is symmetrical about the storm center (Ekman suction). Cold Wake asymmetry has been so far mainly attributed to the resonant regime between wind forcing and near-inertial current oscillations on the right side of the track [*Price*, 1981; *Samson et al.*, 2009]. Mixing-induced cooling is indeed the main contributor to the cooling asymmetry for weak and intermediate *WPi* categories (Figures 13g and 13h). For the strongest *WPi* category, mixing-induced cooling asymmetry is however not as prominent, essentially because strong *WPi*s are usually associated with slow TCs, which trigger more symmetric CWs (Figure 8). For the strongest *WPi* category, advection explains most of the asymmetric pattern (∼70%; Figures 13f and 13i), and this is true for both slow and fast moving storms (not shown). In this case, mixing is not the only contributor to the cooling asymmetry.
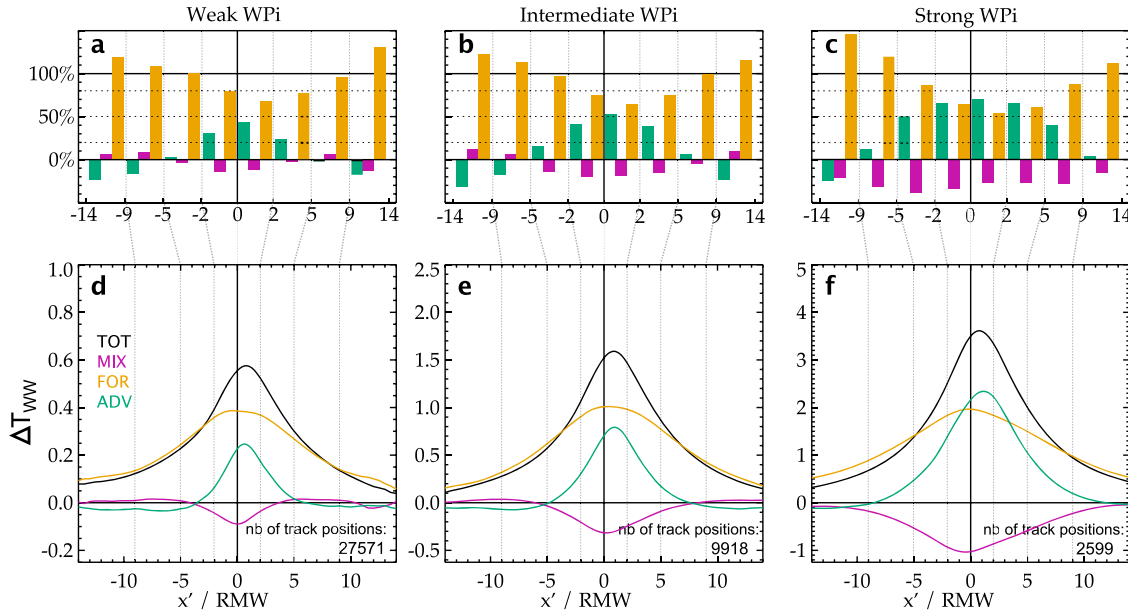
Figure 15. Same as Figures 13a–13f but for the wake warming phase ΔT_{WW} (difference between T_{WW} temperature averaged from day + 3 to day + 63 and T_{CW} in the time integral of each ML heat budget term).

[42] The role of horizontal advection on the CW asymmetry has so far been poorly documented [*Chen et al.*, 2010]. Figure 14a displays separately the along and cross-track advection terms in the frame of the moving TC ($v'\partial_{y'}T$ and $u'\partial_{x'}T$, respectively, with u/x′ the cross-track surface current/axis, and v/y′ the along-track current and axis) for the largest wind forcing. This analysis reveals that asymmetry related to the heat advection mainly results from the along-track component. A two dimensional composite of horizontal currents in the TC-moving frame (Figure 14b) allows understanding this feature. Figure 14 corresponds to a 4-day average, so that near-inertial currents triggered by the TC forcing are largely smoothed (and their residual, i.e., the stationary Ekman flow, is contained in the ageostrophic component). Surface currents anomalies are primarily related to the geostrophic response to the TC-induced negative SSH anomaly under the track (Figure 14b). The negative SSH anomaly centered on the TC position is associated with a cyclonic geostrophic surface circulation (Figure 14b). The ageostrophic part of the current is largely consistent with the stationary Ekman transport response to cyclonic wind forcing (veered to the right of the surface wind stress, Figure 14b).

[43] Along the cross-track axis, geostrophic currents dominate along-track currents (Figure 14d), with forward (backward) currents to the right (left) of the track. This current asymmetry combines with the cold wake asymmetry, with coldest anomalies in the rear-right quadrant (Figure 14b). Along-track currents advect water from the cold wake forward to the right of the track, while they advect relatively warmer water backward on the left side. This explains why along-track currents are a strong source of asymmetry (Figure 14a). As indicated above, cross track currents are dominated by the divergent stationary surface Ekman flow, which is symmetric with respect to the TC-track (Figure 14c). The cross-track component advects cold water from the wake away from the cyclone

track, hence cooling both sides in roughly equal proportions (Figure 14a). Asymmetric effect of the cooling for strong cyclones is hence largely due to forward advection of the cold wake by geostrophic currents to the right of the track.

4.3. Processes Controlling the Cold Wake Damping

[44] The good agreement between the modeled and observed SST during the cold wake dissipation (Figure 7a) suggests that our simulation is able to describe the first-order processes that lead to the CW recovery. Based on the averaged time-series, the value of the e-folding time (time for the cold anomaly to be reduced by a factor *e*) is 15 days, in broad agreement with e-folding scales estimated by *Price et al.* [2008] (5 days for TC Fabian and 20 days for TC Frances). About 60 days after the TC passage, the cold anomaly is almost entirely restored to background conditions. Figure 15 shows the integral of the ML temperature budget terms during the warming phase, averaged over a 60-day period starting 3 days after the storm passage. As expected, air-sea heat flux forcing appears as the main process responsible for the CW damping, explaining more than 80% of the ML warming for weak and intermediate strength *WPi* (Figures 15a and 15b). Lateral advection plays a non-negligible role close to the TC track where it explains more than 30% of the warming (and up to 70% for the strongest and or slowest cyclones, Figures 15c and 15f).

5. Conclusion

5.1. Summary

[45] This paper investigates the processes controlling the sea surface cooling induced by Tropical Cyclones (TCs). To that end, we use an ocean general circulation model forced from reconstructed wind perturbations associated with more than 3000 observed TCs over the 1978–2007 period. Reanalysis products usually used to force ocean models

strongly underestimate the amplitude of TCs wind forcing and the resulting TC-induced cooling. We developed an original methodology that allows realistic TC wind forcing based on an idealized vortex [*Willoughby et al.*, 2006] to be included, constrained by observed TC characteristics (location, amplitude) and applied at each ocean model time step.

[46] The statistics of the simulated ocean surface temperature response to TC compare reasonably well to satellite estimates. Average surface temperature anomaly is ∼1°C and extends typically over 5 radii of maximum wind (RMW). The modeled cold anomaly amplitude also agrees well with observations at individual locations (0.71 correlation), although the model tends to overestimate cold wakes associated with the strongest and slowest TCs. Overall, the good agreement between the model and observations allows us to estimate the contribution of various oceanic processes to TC cooling for a very diverse sample of observed cyclones over 1978–2007, providing a more general insight than case studies.

[47] The amplitude of the TC-induced cooling depends on the strength of the TC forcing. Following Vincent et al. (submitted manuscript, 2011), we use the wind power index (*WPi*) as an integrated measure of the cyclone's wind forcing. *WPi* is a proxy of kinetic energy transferred to the upper ocean by the cyclone, and integrates important parameters for the cold wake amplitude (cyclone size, intensity and translation speed). TC-induced cooling within 200 km of the TC eye increases linearly with *WPi*: vertical mixing at the base of the mixed layer explains from ∼30% of the cooling for weak *WPi* up to ∼80% for large *WPi* (above 2.75). Surface heat fluxes however overcome the mixing contribution for lowest *WPi*s (for *WPi* < 2, surface fluxes contribute to ∼50%–70% of the cold wake). Away from the cyclone's eye, latent heat fluxes contribute increasingly to the cooling: surface fluxes explain 50 to 80% of the weak cooling further than ∼250 km away from the track.

[48] Lateral advection plays a modest role compared to mixing and surface fluxes. For the strongest and/or slowest cyclones, it can however explain up to 30% of the cooling to the right of the TC track. While mixing dominates the cold-wake asymmetry for weak and intermediate *WPi*s, our results suggest that the anti-symmetric pattern of along-track currents is the main contributor to the cooling asymmetry for the most intense cyclones (*WPi* > 4.5). This asymmetry is primarily related to the forward advection of cold wake water by geostrophic currents on the right side of the TC. While heat fluxes control to a large extent the damping of the CW in the months following the TC passage, our analysis also reveals that advective processes play a non-negligible role, contributing to as much as 70% close to the TC track for the strongest TC wind forcing.

[49] The pre-storm ocean state also modulates the amplitude of the TC-induced cooling. The Cooling Inhibition index (CI) is a measure of the ocean "resistance" to cooling by the TC (measured as the amount of potential energy required to cool the ocean surface by 2°C (Vincent et al., submitted manuscript, 2011)). Using this measure, Vincent et al. (submitted manuscript, 2011) showed that ocean background state can modulate the cooling amplitude by up to an order of magnitude for a given cyclone wind power input. We show here that this modulation is related to the increasing efficiency of mixing to cool the ocean surface

when CI decreases. In the case of strong CI, the surface current kinetic energy is dissipated to produce vertical mixing but in this case, little cold water is entrained into the ML. In contrast, weak CI is usually associated to a shallow ML and/or steep temperature stratification below the ML before the TC passage, allowing mixing to efficiently incorporate cold water into the ML.

5.2. Limitations of the Present Study

[50] Although the model response to TCs agrees well with observations, we believe that our modeling strategy can be further improved. An inherent limitation to our study is that we rely on analytical formulations for the RMW and surface wind field of TCs. The latest version of the IBTrACS database provide radius estimations for some cyclones, which could be a first step in defining the geometry of the cyclone better. Using satellite observations of surface TC wind from QSCAT would provide more accurate wind pattern but satellites do not provide accurate estimates of the strongest winds. *Sriver and Huber* [2010] used QSCAT surface winds extracted around observed TC tracks to force an ocean general circulation model; they noted that this method underestimates the observed cooling and had to multiply the wind amplitude by a factor 2 to yield realistic cooling amplitude. By contrast, our strategy is based on observed TCs amplitudes and allows us to accurately represent the amplitude of TC-induced cooling in spite of the rather low resolution of the ocean model. This may be due to the fact that we resolve better temporal variations of the cyclone winds, and hence energy transfers to the upper ocean. We indeed apply wind perturbations every time-step (36 minutes) using an interpolated cyclone position, while QSCAT temporal sampling is at best daily, and a cyclone typically travels over ∼400 km in 1 day.

[51] We have shown that our 1/2° resolution model simulates reasonably the CW magnitude and spatial extent. The simple analysis of Figure 2 indeed suggests that the 1/2° resolution is enough to capture the transfer of cyclone kinetic energy to the upper ocean, which is the main driver of mixing, a dominant process in the cold wake formation. Figure 2 however suggests that Ekman suction maximum amplitude is probably underestimated by ∼30% near the cyclone eye. As demonstrated by several studies [*Greatbatch*, 1985; *Yablonsky and Ginis*, 2009; Jullien et al., submitted manuscript, 2011], Ekman suction can promote increased cooling by shallowing the thermocline near the eye, thus making mixing more efficient. Higher resolution experiments (at least 1/4°) may hence be needed to strengthen the present results. But again, the relatively good agreement between the simulated cold wake and available observations suggest that the current study probably resolves most of the dominant processes.

[52] The wind forcing asymmetry due to the translation speed of TCs has been designated as a secondary order process in regulating the asymmetry of the SST response to TCs [*Price et al.*, 1994; *Samson et al.*, 2009]. We confirm the secondary order importance of this process as the simulation produces asymmetric cold wakes without this effect. We however believe that including this effect may improve characteristics of the simulated CW asymmetry, in particular for fast cyclones.

[53] Cloudiness, precipitation, temperature and humidity anomalies associated to TCs are poorly accounted for in our experimental design. We indeed rely on COREII forcing (i.e., a crude resolution re-analysis) to provide the air temperature and humidity perturbations associated with cyclones, and neglect TC rainfall. Strong uncertainties thus remain on surface fluxes because of air temperature, humidity, and cloud cover perturbations associated with the cyclone. We did not take into account the strong precipitation associated to TC passage either, neglecting the stabilizing effect they may have on the water column and hence potentially overestimate the mixing induced by TCs associated with heavy precipitation.

[54] Finally, mesoscale eddies are known to modulate the ocean response to TCs [*Jacob and Shay*, 2003] and the most intense TCs are often developing over warm core eddies [*Lin et al.*, 2005, 2008] where SST cooling is inhibited. Because our model does not include data assimilation, the position of such eddies in our model is uncorrelated to the observed one. This explains in part why the correlation between simulated and observed cold wakes is "only" 0.71. Moreover, the most intense TCs occur randomly over warm or cold core eddies in our simulation while they tend to occur preferentially over warm core eddies in reality. This sampling discrepancy may be responsible for the overestimation of the average modeled cooling for intense TCs.

5.3. Perspectives

[55] Results described in this paper have practical consequences for statistical operational forecasts of TC intensity. For strongest TC forcing, cooling under the eye is to a large extent controlled by vertical entrainment and mixing. Including an index describing the ocean sub-surface stratification as proposed by Vincent et al. (submitted manuscript, 2011) or *Lloyd and Vecchi* [2011] could hence greatly benefit to cyclone intensity statistical forecast schemes [*DeMaria et al.*, 2005; *Mainelli et al.*, 2008]. However, for weaker cyclones, the effect of surface fluxes cannot be neglected and alternative indices should be proposed to account for their effect on TC-induced cooling.

[56] These results can also be interpreted in the light of the potential impacts of TCs on the ocean at climatic timescales [*Emanuel*, 2001; *Sriver and Huber*, 2010; *Scoccimarro et al.*, 2011]. TC-induced mixing warms water under the ML at the same time as it cools the ML temperature. If surface cold anomaly is entirely damped by surface fluxes, a net warming of the water column results and has to be equilibrated by lateral heat transport [*Emanuel*, 2001]. *Sriver et al.* [2008] argued that TCs significantly modify the poleward heat transport out of the tropics assuming that the observed surface cooling is entirely due to vertical mixing within a 6° footprint around the cyclone. This assumption presumably led the authors to overestimate the amount of heat pumped downward: mixing indeed only explains 52% of the total cooling within 6° of the TC track in our simulation.

[57] Finally, because cooling by surface fluxes affect large areas, we argue that any attempt to diagnose the effects of TCs on the ocean heat budget at the climatic timescale should account for the influence of surface heat fluxes. Further studies are required to investigate the relative effects of mixing and surface fluxes induced by TCs, and their related impacts on the ocean at climatic timescale.

References

Axell, L. B. (2002), Wind-driven internal waves and Langmuir circulations in a numerical ocean model of the southern Baltic Sea, *J. Geophys. Res.*, *107*(C11), 3204, doi:10.1029/2001JC000922.

Barnier, B., et al. (2009), Erratum: Impact of partial steps and momentum advection schemes in a global ocean circulation model at eddy-permitting resolution, *Ocean Dyn.*, *59*, 537, doi:10.1007/s10236-009-0180-y.

Bender, M. A., and I. Ginis (2000), Real-case simulations of hurricane-ocean interaction using a high-resolution coupled model: Effects on hurricane intensity, *Mon. Weather Rev.*, *128*, 917–946, doi:10.1175/1520-0493(2000)128<0917:RCSOHO>2.0.CO;2.

Bender, M. A., I. Ginis, and Y. Kurihara (1993), Numerical simulations of tropical cyclone-ocean interaction with a high-resolution coupled model, *J. Geophys. Res.*, *98*(23), 245–263.

Bernard, B., et al. (2006), Impact of partial steps and momentum advection schemes in a global ocean circulation model at eddy-permitting resolution, *Ocean Dyn.*, *56*, 543–567, doi:10.1007/s10236-006-0082-1.

Brennan, M. J., C. C. Hennon, and R. D. Knabb (2009), The operational use of QuikSCAT ocean surface vector winds at the National Hurricane Center, *Weather Forecasting*, *24*(3), 621–645, doi:10.1175/2008WAF2222188.1.

Burchard, H. (2002), Energy-conserving discretisation of turbulent shear and buoyancy production, *Ocean Modell.*, *4*, 347–361, doi:10.1016/S1463-5003(02)00009-4.

Chen, S., T. J. Campbell, H. Jin, S. Gaberšek, R. M. Hodur, and P. Martin (2010), Effect of two-way air–sea coupling in high and low wind speed regimes, *Mon. Weather Rev.*, *138*, 3579–3602, doi:10.1175/2009MWR3119.1.

Chiang, T. L., C. R. Wu, and L. Y. Oey (2011), Typhoon Kai-Tak: An ocean's perfect storm, *J. Phys. Oceanogr.*, *41*, 221–233, doi:10.1175/2010JPO4518.1.

Cione, J. J., and E. W. Uhlhorn (2003), Sea surface temperature variability in hurricanes: Implications with respect to intensity change, *Mon. Weather Rev.*, *131*, 1783–1796, doi:10.1175//2562.1.

Cione, J. J., P. G. Black, and S. H. Houston (2000), Surface observations in the hurricane environment, *Mon. Weather Rev.*, *128*, 1550–1561, doi:10.1175/1520-0493(2000)128<1550:SOITHE>2.0.CO;2.

D'Asaro, E. A. (2003), The ocean boundary layer below Hurricane Dennis, *J. Phys. Oceanogr.*, *33*, 561–579, doi:10.1175/1520-0485(2003)033<0561:TOBLBH>2.0.CO;2.

D'Asaro, E. A., T. B. Sanford, P. P. Niiler, and E. J. Terrill (2007), Cold wake of Hurricane Frances, *Geophys. Res. Lett.*, *34*, L15609, doi:10.1029/2007GL030160.

de Boyer Montégut, C., G. Madec, A. S. Fischer, A. Lazar, and D. Iudicone (2004), Mixed layer depth over the global ocean: An examination of profile data and a profile-based climatology, *J. Geophys. Res.*, *109*, C12003, doi:10.1029/2004JC002378.

DeMaria, M., M. Mainelli, L. K. Shay, J. A. Knaff, and J. Kaplan (2005), Further improvements to the statistical hurricane intensity prediction scheme (SHIPS), *Weather Forecast.*, *20*, 531–543, doi:10.1175/WAF862.1.

Donelan, M. A., B. K. Haus, N. Reul, W. J. Plant, M. Stiassnie, H. C. Graber, O. B. Brown, and E. S. Saltzman (2004), On the limiting aerodynamic roughness of the ocean in very strong winds, *Geophys. Res. Lett.*, *31*, L18306, doi:10.1029/2004GL019460.

Emanuel, K. A. (1986), An air-sea interaction theory for tropical cyclones. Part I: Steady-state maintenance, *J. Atmos. Sci.*, *43*, 585–605, doi:10.1175/1520-0469(1986)043<0585:AASITF>2.0.CO;2.

Emanuel, K. A. (2001), Contribution of tropical cyclones to meridional heat transport by the oceans, *J. Geophys. Res.*, *106*, 14,771–14,781, doi:10.1029/2000JD900641.

Emanuel, K. A. (2003), Tropical cyclones, *Annu. Rev. Earth Planet. Sci.*, *31*, 75–104, doi:10.1146/annurev.earth.31.100901.141259.

Emanuel, K. A. (2005), Increasing destructiveness of tropical cyclones over the past 30 years, *Nature*, *436*, 686–688, doi:10.1038/nature03906.

Greatbatch, R. J. (1983), On the response of the ocean to a moving storm: The nonlinear dynamics, *J. Phys. Oceanogr.*, *13*, 357–367, doi:10.1175/1520-0485(1983)013<0357:OTROTO>2.0.CO;2.

Greatbatch, R. J. (1985), On the role played by upwelling of water in low-ering sea surface temperatures during the passage of a storm, *J. Geophys. Res.*, *90*, 11,751–11,755, doi:10.1029/JC090iC06p11751.

Griffies, S., et al. (2009), Coordinated ocean-ice reference experiments (COREs), *Ocean Modell.*, *26*, 1–46, doi:10.1016/j.ocemod.2008.08.007.

Halliwell, G. R., L. K. Shay, J. K. Brewster, and W. J. Teague (2011), Eval-uation and sensitivity analysis of an ocean model response to Hurricane Ivan, *Mon. Weather Rev.*, *139*, 921–945, doi:10.1175/2010MWR3104.1.

Huang, P., T. B. Sanford, and J. Imberger (2009), Heat and turbulent kinetic energy budgets for surface layer cooling induced by the passage of Hur-ricane Frances (2004), *J. Geophys. Res.*, *114*, C12023, doi:10.1029/2009JC005603.

Jacob, S. D., and L. K. Shay (2003), The role of oceanic mesoscale features on the tropical cyclone-induced mixed layer response: A case study, *J. Phys. Oceanogr.*, *33*, 649–676, doi:10.1175/1520-0485(2003)33<649:TROOMF>2.0.CO;2.

Jacob, S. D., L. K. Shay, A. J. Mariano, and P. G. Black (2000), The 3D oceanic mixed layer response to Hurricane Gilbert, *J. Phys. Oceanogr.*, *30*, 1407–1429, doi:10.1175/1520-0485(2000)030<1407:TOMLRT>2.0.CO;2.

Jansen, M. F., R. Ferrari, and T. A. Mooring (2010), Seasonal versus per-manent thermocline warming by tropical cyclones, *Geophys. Res. Lett.*, *37*, L03602, doi:10.1029/2009GL041808.

Kaplan, J., and M. DeMaria (2003), Large-scale characteristics of rapidly intensifying tropical cyclones in the North Atlantic Basin, *Weather Fore-casting*, *18*, 1093–1108.

Knapp, K. R., M. C. Kruk, D. H. Levinson, H. J. Diamond, and C. J. Neumann (2010), The International Best Track Archive for Climate Stewardship (IBTrACS): Unifying tropical cyclone data, *Bull. Am. Meteorol. Soc.*, *91*, 363–376, doi:10.1175/2009BAMS2755.1.

Large, W., and S. Yeager (2009), The global climatology of an interannu-ally varying air–sea flux data set, *Clim. Dyn.*, *33*, 341–364, doi:10.1007/s00382-008-0441-3.

Leipper, D. F. (1967), Observed ocean conditions and Hurricane Hilda, 1964, *J. Atmos. Sci.*, *24*, 182–186, doi:10.1175/1520-0469(1967)024<0182:OOCAHH>2.0.CO;2.

Lévy, M., A. Estublier, and G. Madec (2001), Choice of an advection scheme for biogeochemical models, *Geophys. Res. Lett.*, *28*(19), 3725–3728, doi:10.1029/2001GL012947.

Lin, I. I., C. C. Wu, K. A. Emanuel, I. H. Lee, C. R. Wu, and I. F. Pun (2005), The interaction of Supertyphoon Maemi (2003) with a warm ocean eddy, *Mon. Weather Rev.*, *133*, 2635–2649, doi:10.1175/MWR3005.1.

Lin, I. I., C. C. Wu, I. F. Pun, and D. S. Ko (2008), Upper-ocean thermal structure and the western North Pacific category 5 typhoons. Part I: Ocean features and the category 5 typhoons' intensification, *Mon. Weather Rev.*, *136*, 3288–3306, doi:10.1175/2008MWR2277.1.

Liu, L. L., W. Wang, and R. X. Huang (2008), The mechanical energy input to the ocean induced by tropical cyclones, *J. Phys. Oceanogr.*, *38*, 1253–1266, doi:10.1175/2007JPO3786.1.

Lloyd, I. D., and G. A. Vecchi (2011), Observational evidence of oceanic controls on hurricane intensity, *J. Clim.*, *24*, 1138–1153, doi:10.1175/2010JCLI3763.1.

Locarnini, R. A., et al. (2010), *World Ocean Atlas 2009*, vol. 1, *Tempera-ture*, NOAA Atlas NESDIS, vol. 68, edited by S. Levitus, NOAA, Silver Spring, Md.

Madec, G. (2008), NEMO ocean engine, *Note Pôle Modél. 27*, Inst. Pierre-Simon Laplace, Paris.

Mainelli, M., M. DeMaria, L. K. Shay, and G. Goni (2008), Application of oceanic heat content estimation to operational forecasting of recent Atlan-tic category 5 hurricanes, *Weather Forecasting*, *23*, 3–16, doi:10.1175/2007WAF2006111.1.

Marks, F., et al. (1998), Landfalling tropical cyclones: Forecast problems and associated research opportunities, *Bull. Am. Meteorol. Soc.*, *79*, 305–323.

Marsaleix, P., et al. (2008), Energy conservation issues in sigma-coordinate free-surface ocean models, *Ocean Modell.*, *20*, 61–89, doi:10.1016/j.ocemod.2007.07.005.

Mellor, G., and A. Blumberg (2004), Wave breaking and ocean surface layer thermal response, *J. Phys. Oceanogr.*, *34*(3), 693–698, doi:10.1175/2517.1.

Morey, S. L., M. A. Bourassa, D. S. Dukhovskoy, and J. J. O'brien (2006), Modeling studies of the upper ocean response to a tropical cyclone, *Ocean Dyn.*, *56*, 594–606, doi:10.1007/s10236-006-0085-y.

Penduff, T., et al. (2010), Impact of global ocean model resolution on sea-level variability with emphasis on interannual time scales, *Ocean Sci.*, *6*, 269–284, doi:10.5194/os-6-269-2010.

Pollard, R., P. Rhines, and R. Thompson (1973), The deepening of the wind-mixed layer, *Geophys. Fluid Dyn.*, *3*, 381–404.

Price, J. F. (1981), Upper ocean response to a hurricane, *J. Phys. Oceanogr.*, *11*, 153–175, doi:10.1175/1520-0485(1981)011<0153:UORTAH>2.0.CO;2.

Price, J. F., T. B. Sanford, and G. Z. Forristall (1994), Forced stage response to a moving hurricane, *J. Phys. Oceanogr.*, *24*, 233–260, doi:10.1175/1520-0485(1994)024<0233:FSRTAM>2.0.CO;2.

Price, J. F., J. Morzel, and P. P. Niiler (2008), Warming of SST in the cool wake of a moving hurricane, *J. Geophys. Res.*, *113*, C07010, doi:10.1029/2007JC004393.

Samson, G., H. Giordani, G. Caniaux, and F. Roux (2009), Numerical investigation of an oceanic resonant regime induced by hurricane winds, *Ocean Dyn.*, *59*, 565–586, doi:10.1007/s10236-009-0203-8.

Sanford, B., et al. (1987), Ocean response to a hurricane. Part I: Observa-tions, *J. Phys. Oceanogr.*, *17*, 2065–2083, doi:10.1175/1520-0485(1987)017<2065:ORTAHP>2.0.CO;2.

Schade, L. R. (2000), Tropical cyclone intensity and sea surface tempera-ture, *J. Atmos. Sci.*, *57*, 3122–3130, doi:10.1175/1520-0469(2000)057<3122:TCIASS>2.0.CO;2.

Schade, L. R., and K. A. Emanuel (1999), The ocean's effect on the inten-sity of tropical cyclones: Results from a simple coupled atmosphere–ocean model, *J. Atmos. Sci.*, *56*, 642–651, doi:10.1175/1520-0469(1999)056<0642:TOSEOT>2.0.CO;2.

Scoccimarro, E., S. Gualdi, A. Bellucci, A. Sanna, P. G. Fogli, E. Manzini, M. Vichi, P. Oddo, and A. Navarra (2011), Effects of tropical cyclones on ocean heat transport in a high resolution coupled general circulation model, *J. Clim.*, *24*, 4368–4384, doi:10.1175/2011JCLI4104.1.

Shay, L. K., and J. K. Brewster (2010), Oceanic heat content variability in the eastern Pacific Ocean for hurricane intensity forecasting, *Mon. Weather Rev.*, *138*, 2110–2131, doi:10.1175/2010MWR3189.1.

Shay, L. K., P. Black, A. Mariano, J. Hawkins, and R. Elsberry (1992), Upper ocean response to Hurricane Gilbert, *J. Geophys. Res.*, *97*(20), 227–248.

Shay, L. K., G. J. Goni, and P. G. Black (2000), Effects of a warm oceanic feature on Hurricane Opal, *Mon. Weather Rev.*, *128*, 1366–1383, doi:10.1175/1520-0493(2000)128<1366:EOAWOF>2.0.CO;2.

Shen, W., and I. Ginis (2003), Effects of surface heat flux-induced sea sur-face temperature changes on tropical cyclone intensity, *Geophys. Res. Lett.*, *30*(18), 1933, doi:10.1029/2003GL017878.

Sriver, R. L., and M. Huber (2010), Modeled sensitivity of upper thermo-cline properties to tropical cyclone winds and possible feedbacks on the Hadley circulation, *Geophys. Res. Lett.*, *37*, L08704, doi:10.1029/2010GL042836.

Sriver, R. L., M. Huber, and J. Nusbaumer (2008), Investigating tropical cyclone-climate feedbacks using the TRMM Microwave Imager and the Quick Scatterometer, *Geochem. Geophys. Geosyst.*, *9*, Q09V11, doi:10.1029/2007GC001842.

Vialard, J., C. E. Menkes, J.-P. Boulanger, P. Delecluse, and E. Guilyardi (2001), A model study of oceanic mechanisms affecting equatorial Pacific sea surface temperature during the 1997–98 El Niño, *J. Phys. Oceanogr.*, *31*, 1649–1675, doi:10.1175/1520-0485(2001)031<1649:AMSOOM>2.0.CO;2.

Vialard, J., et al. (2009), Cirene: Air sea interactions in the Seychelles-Chagos thermocline ridge region, *Bull. Am. Meteorol. Soc.*, *90*, 45–61, doi:10.1175/2008BAMS2499.1.

Wentz, F. J., C. Gentemann, D. Smith, and D. Chelton (2000), Satellite measurements of sea surface temperature through clouds, *Science*, *288*, 847–850, doi:10.1126/science.288.5467.847.

Willoughby, H. E., and M. E. Rahn (2004), Parametric representation of the primary hurricane vortex. Part I: Observations and evaluation of the Hol-land (1980) Model, *Mon. Weather Rev.*, *132*, 3033–3048, doi:10.1175/MWR2831.1.

Willoughby, H. E., R. W. R. Darling, and M. E. Rahn (2006), Parametric representation of the primary hurricane vortex. Part II: A new family of sectionally continuous profiles, *Mon. Weather Rev.*, *134*, 1102–1120, doi:10.1175/MWR3106.1.

Yablonsky, R. M., and I. Ginis (2009), Limitation of one-dimensional ocean models for coupled hurricane-ocean model forecasts, *Mon. Weather Rev.*, *137*, 4410–4419, doi:10.1175/2009MWR2863.1.

N. C. Jourdain, LEGI, CNRS/UJF/INPG, BP 53, Grenoble F-38401 CEDEX 09, France.

S. Jullien, LEGOS, IRD/CNRS/UPS, 18, Ave. Edouard Belin, Toulouse F-31401 CEDEX 09, France.

M. Lengaigne, G. Madec, G. Samson, J. Vialard, and E. M. Vincent, LOCEAN, IRD/CNRS/UPMC/MNHN, Tour 45-55 4ème 4, Place Jussieu, Paris F-75252 CEDEX 05, France. (emvincent@phare.normalesup.org)

C. E. Menkes, IRD, 101 Promenade Roger Laroque, BP A5, 98848 Noumea, New Caledonia.